AN ABSTRACT OF THE THESIS OF

Annalise Miller for the degree of Master of Science in Mechanical Engineering presented on June 8, 2018.

Title: Advancing Wind Systems Design through Optimization and Improved Modeling

approved: _____

Bryony L. DuPont

Wind energy plays an important and growing role in the US energy profile. While other countries have expanded their wind industries into offshore development, large investment costs have hindered progress in the US offshore market despite the larger and more consistent resource available offshore. In this research, I explore the optimization of floating offshore farms specific to the US west coast, with the goal of curbing currently prohibitive monetary barriers to market expansion. I begin by selecting the best optimization algorithm for the offshore wind farm layout problem using a simplified wind case. I then compare the optimization of onshore and offshore wind farms under both simplified and more realistic wind scenarios. My third study explores the trade-offs between the accuracy and computational expense of high-fidelity computational fluid dynamics wake models and the lower-fidelity, linearized PARK model (a common analytical representation of wind turbine wake interactions). Finally, I analyze the performance differences as a result of turbine manufacturer through a turbine availability analysis of two turbine vendors. Results from this study implicate best practices for onshore and offshore wind farm optimization pertaining to algorithm type, wake model selection, and turbine manufacturer. This information may be used by developers and policy makers to inform decision making and increase profits and farm-wide power production.

Advancing Wind Systems Design through Optimization and Improved Modeling

by

Annalise Miller

A THESIS

submitted to

Oregon State University

in partial fulfillment of
the requirements for the
degree of

Master of Science

Presented June 8, 2018
Commencement June 2018

Master of Science thesis of Annalise Miller presented on June 8, 2018

APPROVED:

Major professor, representing Mechanical Engineering

Head of the School of Mechanical, Industrial, and Manufacturing Engineering

---

Dean of the Graduate School

I understand that my thesis will become part of the permanent collection of Oregon State University libraries. My signature below authorizes release of my thesis to any reader upon request.

Annalise Miller, Author

ACKNOWLEDGEMENTS

To Kenny Martin for specifically not telling me that aspiring to build treehouses powered through micro-renewables is impractical. And for treating me as a competent adult when I came to office hours wearing a daisy chain crown.

To my committee, all of whom I have worked with through research and classes.

To Kyle Niemeyer, for helping me through funding and coding hurdles. I certainly owe you a beer.

To Bryony, who took me on as a graduate student despite a moderate lack of direction. I still haven't figured out why you did it, but I'm certainly grateful that you did!

To my family, who don't always know why I do the things I do, but seldom question it. Thanks guys!

To Sheila, the most honest and loving friend. Who is not afraid to laugh at you when you deserve it. Thanks for keeping me honest.

To the 910 house, I miss you all.

To Mick. The best. My favorite. Mine.

TABLE OF CONTENTS

TABLE OF CONTENTS (Continued)

TABLE OF CONTENTS (Continued)

LIST OF FIGURES

LIST OF FIGURES (Continued)

LIST OF TABLES

ADVANCING WIND SYSTEMS DESIGN THROUGH OPTIMIZATION AND IMPROVED MODELING

1 INTRODUCTION

1.1 The Role of Wind Energy in the US

International energy demand is projected to increase by 28% by 2040. The Energy Information Administration projects that renewable energy will be the fastest-growing energy source in meeting this future demand with average annual increases of 2.8% [5]. Wind energy accounted for 21% of US renewable energy generation in 2016 [6]. By the third quarter of 2017 the US had nearly 85 GW of installed wind energy capacity dispersed among 41 states and accounting for $143 billion invested in the last 10 years [7].

1.2 The Expanding Role of Offshore Wind Energy

The large wind resource off the west coast of the United States has the potential to generate wind power for millions of homes, yet the high cost of energy for offshore wind power (compared to traditional sources) has hindered the development of offshore wind farms in the US. Despite these costs, it is predicted that by 2030, there will be 54 MW of offshore wind energy installed domestically [8]. Multiple proposed and ongoing offshore wind projects exist in the US, the majority of which are for developments off the US East Coast, where the bathymetry is shallow [8]. The bulk of this research focuses instead on potential developments off the US Pacific Coast. The steep bathymetry and

deep waters off the West Coast make it infeasible to install embedded, bottom-fixed wind farms. Instead I explore the use of more expensive floating turbine foundations, made feasible by increased revenue from the larger (estimated 900 GW) and more predictable Pacific coast wind resource [9, 10, 11].

Floating platforms supporting large wind turbines in deep ocean waters are modeled after floating oil and gas rigs [12]. While many types of floating platforms have been proposed, the three most common designs are the spar-buoy, the tension leg-platform (TLP), and the semi-submersible platform. A selection of offshore wind farm platform types are shown in Fig. 1.1. A semi-submersible platform called WindFloat, designed by Principle Power, had been installed off the coast of Portugal, and supports a 2 MW wind turbine [12]. Another project using the WindFloat design, called WindFloat Pacific, was zoned off the US West Coast, where a 30 MW array was to be installed near Coos Bay, Oregon (the project has since moved to Northern California) [13, 14]. In this research, I explore the layout of commercial-scale wind turbines using WindFloat platforms, on the basis of these real-world implementations.

Floating offshore wind installations have high investment and operations and maintenance (O&M) costs that can be prohibitive. Therefore, reducing the cost of a floating offshore wind development is crucial for advancing the floating offshore wind power industry in the United States. While initial capital investments are inherently higher for offshore wind farms, a lifetime cost and revenue assessment may reveal economic opportunity in offshore development. For example, differences in wake propagation resulting from varied surface roughness and atmospheric conditions affect power generation and may result in increased revenue in excess of increased costs with consequent adjustments in optimal turbine positioning. There is limited existing research incorporating the floating wind farms necessary to capture the large wind resource in deeper waters.

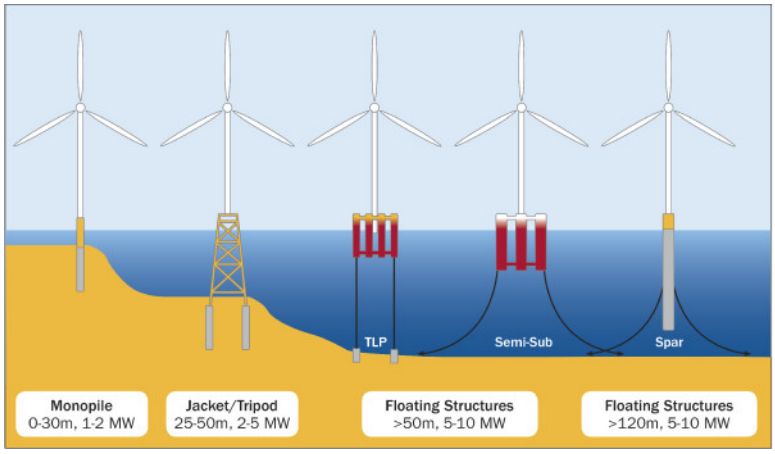

FIGURE 1.1: Offshore Wind Farm Foundation Types from [1]

1.3 Problems Faced by the Wind Industry and Addressed in this Work

While wind energy is becoming more abundant and cost competitive, the industry faces challenges on the pre-development side. Industry profits increase with energy development. In order to develop farms that produce the most power, and thus profit, developers must use accurate models and effective optimization algorithms. In this work I make advances in both of these areas by looking first at identifying the most appropriate optimization algorithm for wind farm layout optimization, and then delving into a comparison of turbine wake model accuracy. Finally, I examine turbine performance data to inform developer assumptions on turbine availability.

To identify the most appropriate algorithm for wind farm optimization, I apply three optimization algorithms to the same, simplified problem formulation. The farm itself is a square, and the ambient wind is a constant speed and originates from a single direction. I apply the algorithms to optimize farms with increasing numbers of turbines to determine the algorithm that best balances the production of optimal turbine layouts with minimized computational expense.

My next two studies explore the optimization of onshore and offshore wind farms

under simplified wind conditions and expand the offshore optimization to a more realistic wind scenario. These studies were designed to provide a better understanding of the unique characteristics of optimized offshore wind farms so as to minimize the farm's cost while maximizing power production.

A third study focuses on the input wake models used in optimization. While there are many wake models available to determine wind speeds at downstream turbines, each model faces a trade-off between accuracy and computational expense. This study compares a simple, linearized wake model commonly used in wind farm optimization with a high-fidelity computational fluid dynamics (CFD) model to determine whether higher accuracy models need to be applied earlier in the wind farm design process.

Finally I conduct a study of turbine availability across a US fleet including 38 farms. I use data from these farms to determine whether turbines from different manufacturers show statistically significant differences in turbine availability. This study allows wind farm developers to make more informed decisions regarding future development.

In the following chapters (Chapters 2 and 3), I discuss the existing research motivating these studies, and provide detail on the cost and wake models used.

2 PREVIOUS APPROACHES

There has been research in seven different topic areas contributing to and motivating this research. Those topic areas are explored in the following subsections.

2.1 Cost Models for Fixed Offshore Wind Farms

Several cost models have been developed to assess offshore wind farms with fixed, monopile foundations. Elkinton et al. developed models that can be applied to any heuristic optimization algorithm for offshore wind farms (using bottom-fixed turbines) that maximize power and minimize cost [15, 16]. Elkinton used an objective function that minimizes the Levelized Cost of Energy (LCOE) and found that Genetic Algorithms and Greedy Heuristic Algorithms were the most viable optimization methods for the offshore wind farm layout problem. Forinash developed a cost model specific to floating offshore wind farms using the Wind Float semi-submersible platform [17]. As my research focuses on modeling floating offshore wind farms, I use the cost model developed by Forinash in this research [17].

2.2 Case Studies in Offshore Wind Modeling

Several wind farm studies focus on quantifying the wind resource and economic incentives at one or more specific farm locations. Mahdy and Bahaj compare onshore and offshore wind resource quantification measures to develop a standardized wind resource assessment procedure that they test using offshore wind data in Egypt [18]. Soares et al. use climate modeling to estimate changes in wind resources associated with the effects of climate change in the waters surrounding the Iberian Peninsula [19]. Chang and Lai

conducted an offshore wind farm optimization at two sites off the coast of Taiwan [20]. This study maximized energy production at various water depth ranges, but did not account for farm costs. Satir et al. analyzed policy based economic incentives and wind resource in Turkey to select farm sites and optimize turbine spacing for gridded layouts at two locations in the Aegean Sea [21]. Kirchner-Bossi and Porté-Agel conducted an optimization of the *Horns Rev I* fixed offshore wind farm using an evolutionary algorithm to minimize wake interactions [22]. While these studies are foundational in understanding offshore wind farm modeling, the research presented in this thesis expands on these approaches by focusing on floating, deep-water solutions instead of shallow-water installations.

2.3 Gradient-Based Optimization of Wind Farms

Gradient-based optimization methods have been used to optimize onshore wind farm layouts. Stanley et al. used a gradient-based method to optimize wind farms with two distinct rotor heights [23]. The algorithm resulted in a 5–9% reduction in the cost of energy when compared to farms with a single turbine height. King et al. used an adjoint optimization method in conjunction with a Reynolds-Averaged Navier–Stokes wake simulation to optimize the Annual Energy Production (AEP) of onshore wind farms [24]. The gradient based algorithm was essential in reducing the computational expense of optimization so as to incorporate the highly expensive high-fidelity CFD wake model. While both studies were able to improve upon their initial layouts, gradient-based optimization is more susceptible to convergence on local optima. Heuristic optimization methods are more computationally expensive than gradient-based approaches, and still not guaranteed to converge on global optima. However, they are less likely to return poor-performing local optima in the highly multi-modal objective space resulting from optimization over multiple objective functions (e.g., cost and power). Because I am considering a multi-modal space with the incorpo-

ration of multiple objectives, I focus my work on the heuristic optimization of floating offshore wind farms that is more suited to this space.

2.4 Wind Farm Optimization Using Genetic Algorithms

Genetic Algorithms (GAs) are optimization techniques based on the processes of evolution and natural selection. In its application to wind farm optimization, a single farm layout is encoded in a binary string, representing a discretized farm. To search the solution space, layouts are "mated" through random crossover wherein a point is selected in the length of the binary strings representing two farms. The end of each original string is replaced with the end of the string it is mated with. Additionally, random mutation may be applied to GAs by selecting a random bit in the string, and replacing it with the opposite binary representation. More on how GAs are used in this work can be found in Section 4.2.

Genetic Algorithms have been the most common technique for offshore wind farm layout optimization. Stochastic algorithms, such as GAs, increase the likelihood of convergence on good solutions in multi-modal systems such as the offshore wind farm layout problem. However, GAs traditionally require the placement of turbines in discrete locations, limiting possible layout combinations. Gao et al. found that scattered layouts optimized using a Multi-Population GA resulted in a higher AEP than aligned or staggered layouts [25, 26]. An offshore wind farm optimization developed by Réthorè et al. included electrical grid and foundation costs as well as energy production. This multi-fidelity model approach combined 1000 iterations of a Simple GA with 20 iterations of a Sequential Linear Programming method applied to a case study in Denmark to develop an improved layout of the Middelgrunden Wind Farm [27]. The approach was found to reduce the computational cost of optimization. Liu and Wang developed an Adapted GA method

that replaces the location swaps of traditional GAs with random crossovers; a wind farm containing 16 turbines in a unidirectional, single wind speed case was optimized to 100% efficiency using this method [28]. I use Liu and Wang's study to validate the functionality of the Extended Pattern Search discussed later in this work.

2.5 Other Optimization Methods Used in Fixed Offshore Wind

Additional heuristic optimization methods for multi-modal spaces have been applied to the offshore wind farm layout optimization problem. Rivas et al. developed a Simulated Annealing Algorithm that employed three local search operations; their algorithm increased the predicted AEP of the Horns Rev offshore wind farm by 1% [29]. Using a Coral Reef Optimization Algorithm, Salcedo-Sanz et al. improved offshore wind farm performance over other approaches, including Evolutionary Algorithms, Differential Evolution Algorithms, and Harmony Search Algorithms[30]. A Viral Based Algorithm with an objective function of Cost of Energy (COE) was developed by Ituarte et al. that decreased COE for a 30-turbine farm, as compared to the GA-derived optimal onshore wind farm layout reported by Mosetti et al. [31, 32]. While a number of heuristic optimization algorithms have been applied to the offshore wind farm optimization problem, few have been applied to floating offshore wind systems, and each optimization problem formulation has used different environmental and optimization parameters. To better compare algorithms directly, I conduct an optimization using the same environmental variables and similar optimization parameters.

2.6 Optimization of Floating Offshore Wind

While fixed-foundation offshore wind farm optimization is becoming more prevalent in research, limited effort has been directed at floating offshore systems. Rodrigues et al. undertook one of the first approaches to the optimization of offshore floating wind farms. They developed a Covariance Matrix Adaptation Evolutionary Strategy (CMA-ES) in a nested configuration to optimize the layout of a floating offshore wind farm comprised of IDEOL platforms supporting 5 MW turbines [33, 34]. This method can optimize layouts in a continuous space for both stationary and movable platforms. Results from the stationary case showed a decrease in Levelized Production Cost (LPC) of 4.17% over a non-optimized grid layout. Pérez et al. developed a two-step sequential optimization procedure that combines a heuristic method to set a random initial layout with nonlinear mathematical programming techniques that search the space to find local optima [35]. This method was applied to the Alpha Ventus offshore wind farm and, compared to the real layout, increased the Annual Energy Production (AEP) by 3.76%. Building on these approaches, this research focuses on WindFloat semi-submersible turbine platforms, with environmental conditions suited specifically to the US Pacific Coast.

2.7 Implementations of the Extended Pattern Search

Pattern Search methods are deterministic heuristic optimization algorithms. Deterministic optimization may work well in monotonic solution spaces, but often converge at poor performing local optima in multi-modal spaces. Stochastic extensions of pattern search algorithms (Extended Pattern Searches) have been shown to increase the efficacy of pattern search algorithms in onshore wind farm optimization [36, 37, 38, 39]. The Extended Pattern Search (EPS) is a moderately stochastic method well-suited for large, multi-modal

systems such as the offshore floating wind farm layout optimization problem. The EPS has shown superior performance to a simulated annealing algorithm in an analogous packing study [40], yielding equivalent or better solutions in fewer objective evaluations.

2.8 Summary of Previous Approaches

Previous research in offshore wind farm optimization has generally concentrated on wind farms consisting of bottom-fixed turbines. Common optimization methods focus on maximizing power output and efficiency of wind farms, with some methods minimizing cost as well. This research expands on the existing work by focusing on the floating offshore wind farm optimization with site parameters characteristic of the US Pacific Coast.

3 WIND FARM MODELING

To properly assess wind farms one must be able to evaluate farm wide power development and costs. This section introduces the wake models and cost models used for these calculations in this research.

3.1 Power Model

The total power produced by a wind farm is taken as the sum of the power produced by each wind turbine. This relationship is shown in Eq. (3.1).

$$P_{tot} = \sum_{i=1}^{n} P_{turb} \tag{3.1}$$

In this equation P_{turb} is the power developed by each individual turbine, and n is the number of turbines in the system.

The power produced by individual turbines is represented by the turbine's power curve; turbines of different sizes have different power curves. An example of a typical power curve is given in Fig. 3.1.

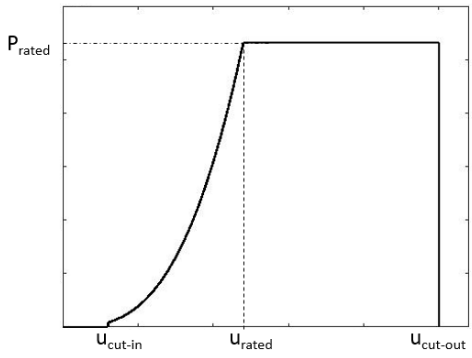

FIGURE 3.1: Generic Wind Turbine Power Curve

This curve is modeled using the piece-wise function in Eq. (3.2). Here, the power production is 0 for wind speeds below cut-in wind speed or above cut-out wind speed. A turbine's rated power is produced at wind speeds between rated wind speed and cut-out wind speed. Between cut-in wind speed and rated wind speed, the power production curve is modeled using a modification from Maxwell et al. [41]. This modification accounts for turbine down time using the η coefficient in Eq. (3.2).

$$Power_i = \begin{cases} 0 & \text{if } u_i < u_{cut-in} \\ \frac{1}{2}\rho A C_p u_i^3 \eta & \text{if } u_i \geq u_{cut-in} \text{ and } u_i < u_{rated} \\ Power_{rated} & \text{if } u_i \geq u_{rated} \text{ and } u_i < u_{cut-out} \\ 0 & \text{if } u_i \geq u_{cut-out} \end{cases} \tag{3.2}$$

Here ρ is air density, C_p is the power coefficient measuring the efficiency of the turbine, A is the rotor swept area of the turbine, u_i is the effective wind speed at the turbine rotor, and η is a measure of the percentage of time a turbine is fully operational.

3.2 Wake Models

There are a variety of wake models that have been used in wind farm optimization. Linearized models, like the PARK model, are appealing for their low computational expense, however these models are typically lower fidelity. Computational fluid dynamics (CFD) models have higher fidelity, but come at the cost of much greater computational expense. Most case studies in this work use the PARK wake model for its low computational expense and high average accuracy [42]. The final study in this work compares the accuracy of the PARK wake model and a Reynolds-Averaged Navier–Stokes CFD model. This section details those wake models.

3.2.1 PARK Model

In this work I use the two-dimensional and a three-dimensional extrapolation of the PARK Wake Model to calculate wind speeds at turbines located in the wakes of upstream turbines [36, 43]. This section outlines the three-dimensional extrapolation of the PARK model.

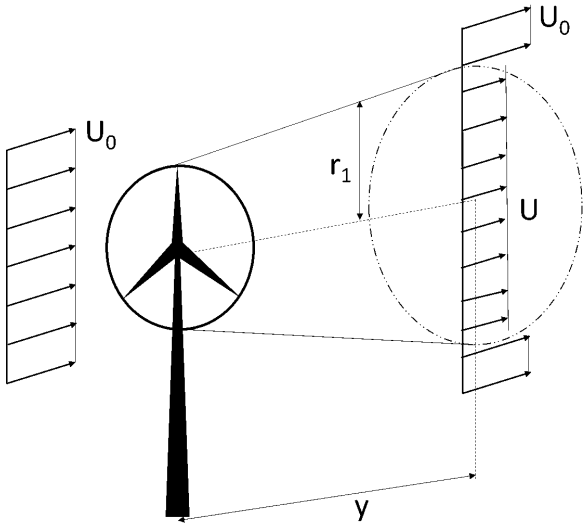

FIGURE 3.2: Three Dimensional Wake Propagation Model [2]

As rotating blades of wind turbines extract energy from the wind, a conical wake is created that propagates downstream (Fig. 3.2). While the air flow immediately behind the rotor is turbulent and the wind speed is greatly reduced from the ambient wind speed, the wake effect will dissipate as it moves downstream. The wind speed downstream of the rotor, U, is calculated using Eq. (3.3):

$$U = U_o \left[1 - \frac{2}{3} \left(\frac{r_r}{r_r + \alpha y} \right)^2 \right] \tag{3.3}$$

where U_o is the ambient wind speed, r_r is the rotor radius of the upstream turbine, y is the distance downstream of the rotor, and α is the entrainment constant (Eq. (3.4)):

$$\alpha = \frac{0.5}{\ln \frac{z}{z_o}} \tag{3.4}$$

where z is the turbine's hub height and z_0 is the farm's surface roughness. If a turbine's rotor is only partially in a wake, or in multiple wakes, the wind speed is a summation of the percentage of the rotor radius in each wake (Fig. 3.3). The equations to calculate the wind speed at rotors with partial and overlapping wakes are derived by DuPont et al. [36, 39].

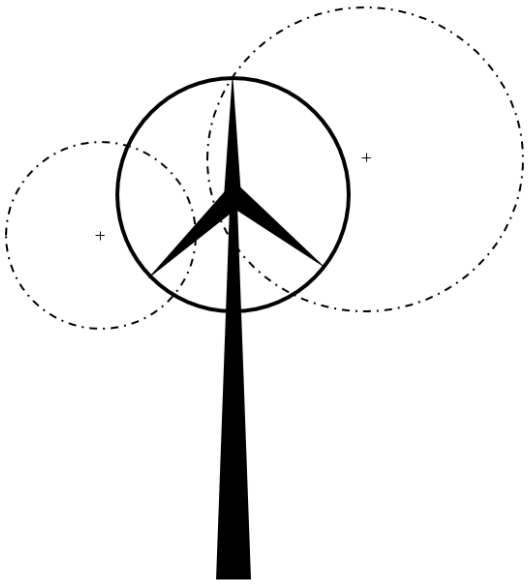

FIGURE 3.3: Interaction of Multiple Wakes within the Rotor Swept Area of a Downstream Turbine [2]

The overlapping wake model begins by calculating the distance between the hub of the downstream turbine and the center line of the wake in question through Eq. (3.5).

$$d_{r-w} = \sqrt{(x_t - x_w)^2 + (z_t - z_w)^2} \tag{3.5}$$

where x_t and x_w are the x–coordinates of the turbine hub and center line of wake respectively, and z_t and z_w are the z–coordinates at the turbine hub and wake center line. A

turbine is in the wake of a second turbine if d_{r-w} is less than the sum of the wake radius, r_w, and turbine rotor radius, r_r (Eq. (3.6)).

$$d_{r-w} < r_r + r_w \tag{3.6}$$

Eq. (3.7) is used to determine the area of overlap between a wake and its downstream turbine, and Eq. (3.8) is used to convert that area into a percentage of the entire rotor swept area.

$$\begin{aligned} A_{overlap} = r_r^2 \arccos\left(\frac{d_{r-w}^2 + r_r^2 - r_w^2}{2d_{r-w}r_r}\right) + r_w^2 \arccos\left(\frac{d_{r-w}^2 + r_w^2 - r_r^2}{2d_{r-w}r_w}\right) \\ -\frac{1}{2}\sqrt{(-d_{r-w}+r_r+r_w)(d_{r-w}+r_r-r_w)(d_{r-w}-r_r+r_w)(d_{r-w}+r_r+r_w)} \end{aligned} \tag{3.7}$$

$$\% = \frac{A_{Overlap}}{\pi r^2} \tag{3.8}$$

Once the rotor swept area of a turbine has been subdivided by level of wake interaction, the power developed in each subdivision is calculated using Eq. (3.2), and the total power produced is the sum of power produced in each subdivision weighted by the percentage of wake overlap from Eq. (3.8).

In the event of multiple wakes overlapping, the rotor swept area is discretized into 49 equally spaced points, and wind speeds are calculated at each point based on the effects of upstream turbines. The wind speed at the downstream turbine is taken to equal the average of the wind speed at each of its 49 discretized points.

Nested Wake Provision

I use a nested wake provision in select case studies throughout this work. The nested wake provision identifies downstream turbines that are entirely within the wake of multiple upstream turbines. Eq. (3.3) is used to determine the wind speed at these downstream turbines, but replace U_o with the wind speed at the closest upstream turbine. This provision helps to account for overestimated wake losses in nested scenarios [44].

3.2.2 CFD Model

In the final study of this research, I compare the accuracy of the PARK wake model to that of a high-fidelity two-dimensional CFD wake model. To make this comparison I use a pre-release version of the WindSE2D software developed by the National Renewable Energy Laboratory [45, 24]. The WindSE2D software uses the fenics program to set up CFD analysis. The primary inputs, in addition to the wind onset angle, wind speed, and turbine locations, are the length and with of the analysis space, the length and width of the farm, and the number of mesh divisions in the analysis space. In these analyses the analysis space is 3–6 times larger in each dimension than the farm space. There are 100 mesh division in the analysis space for all CFD modeling in this work. Further mesh division for all cases in this work were not found to alter the wind speed estimates throughout the farm significantly.

The CFD analysis in this work refines the mesh within the circumradius of the farm using fenics' refine function, applied twice. After the intra-farm mesh refinement, the absolute wake model analysis also refines the the cells of the mesh with 400 m of each turbine once.

3.3 Cost Models

Cost is a primary driver in wind farm development. As such it is imperative to consider costs in the optimization process. This section details the cost models used for onshore and offshore wind farm optimization.

3.3.1 Onshore Cost Model

The cost model employed for onshore wind farm optimization was developed by DuPont et al. [39]. The model estimates a cost surface as a function of turbine rotor radius and hub height based on the National Renewable Energy Laboratory Jobs and

Economic Development Impact model for onshore wind. The onshore farm cost is given by Eq. (3.9).

$$Cost_{Onshore} = Cost_{Project} + Cost_{O\&M} \tag{3.9}$$

where $Cost_{Project}$ is the total project cost, and $Cost_{O\&M}$ is the lifetime sum of operations and maintenance expenditures as outlined in the following sections.

Project Cost

The per-turbine project cost is a function of turbine size given by Eq. (3.10). This equation is valid for certain atmospheric stability conditions that are not explicitly explored in this work.

$$Cost_{Project} = 2.454 \times 10^6 - (2.161 \times 10^5) r_r - (1.203 \times 10^4) h + 6039 r_r^2 + 2455 r_r z - 161.2 z^2 \tag{3.10}$$

where r_r is a turbine's rotor radius and z is a turbine's hub height[39].

Onshore O&M Cost

The onshore O&M costs are a function of energy produced, operational life, capacity factor and cost of energy (COE) as shown in Eq. (3.11) [46]:

$$Cost_{O\&M} = 0.007 * E_y * t * C_f \tag{3.11}$$

where E_y is the yearly energy production in kilowatts, t is the expected lifetime of the farm in years, and C_f is the capacity factor of the farm.

3.3.2 Offshore Cost Model

This work uses the offshore wind farm cost model developed by Forinash and DuPont [17]. The total cost of a floating offshore wind farm is shown in Eq. (3.12).

$$Cost_{total} = Cost_{Capital} + Cost_{Leasing} + Cost_{Mooring} + Cost_{Installation} + Cost_{Substation} + Cost_{Cabling} + Cost_{O\&M} \quad (3.12)$$

The component costs in Eq. (3.12) are expanded in Equations 3.13-3.19 below. In this model P_{rated} is the rated power of the farm in watts, $WCOE$ is the wholesale cost of energy that can be sold back to the grid, *depth* is the water depth at the farm's location, N is the number of turbines on the farm, d_{array} is the length of array cabling necessary to connect the farm's turbines, d_{export} is the necessary cable length to connect the wind farm to the onshore electrical grid, and n_y is the expected life of the wind farm in years.

The capital costs of a wind farm are taken to be \$1.48 per watt as given in Eq. (3.13).

$$Cost_{Capital} = 1.48 * P_{rated} \quad (3.13)$$

The leasing costs of the farm are taken as 2% of the farm's revenue for the first 8 years of operation and 4% of the farm's revenue thereafter. This relationship is shown in Eq. (3.14), where $P_{rated}1 \times 10^6 * 8760 * C_f$ models the energy developed in a given year, $WCOE$ represents the wholesale cost of energy, and $8 * 0.02 + (n_y - 8) * 0.04$ captures the variation in leasing costs over the course of the farm life.

$$Cost_{Leasing} = \frac{P_{rated}}{1 \times 10^6} * 8760 * C_f * WCOE * (8 * 0.02 + (n_y - 8) * 0.04) \quad (3.14)$$

Each floating turbine is assumed to have 4 mooring lines, with a fixed cost of \$140,148 and an additional cost of \$274 per meter depth. The mooring cost of the farm is thus given in Eq. (3.15).

$$Cost_{Mooring} = 4 * (140\,148 + 274 * depth) * N \quad (3.15)$$

Turbine, foundation, mooring, anchoring, and electrical installation of the farm is fixed at $97,762 per turbine as shown in Eq. (3.16).

$$Cost_{Installation} = 97\,762 * N \tag{3.16}$$

Substation costs are $2 million plus $0.02 per watt of rated farm power. This relationship is shown in Eq. (3.17).

$$Cost_{Substation} = 0.02 * P_{rated} + 2 \times 10^6 \tag{3.17}$$

Farm cabling costs consider inter-array and export cabling. Inter-array cabling is modeled at $307 000 per meter and export cabling is modeled at $492 000 per meter. This relationship is shown in Eq. (3.18).

$$Cost_{Cabling} = 307\,000 * d_{array} + 492\,000 * d_{export} \tag{3.18}$$

Farm O&M costs are modeled as $0.133 per watt per year, as shown in Eq. (3.19).

$$Cost_{O\&M} = 0.133 * P_{rated} * n_y \tag{3.19}$$

4 OPTIMIZATION ALGORITHMS

The first step in optimizing wind farms on- or offshore is to determine the appropriate optimization algorithm. The high computational expense of cost and wake models lend themselves logically to gradient based optimization algorithms that converge in few iterations. However, the multimodal objective space created by multi-directional wind conditions and multiple competing objectives leads gradient based algorithms to converge on poor-performing local optima. To better navigate the multi-modal solution space, I have instead elected to move forward with a heuristic optimization approach. Previous studies using a variety of heuristic optimization methods have each used different environmental and experimental inputs as well as optimization parameters that make direct comparison between algorithms difficult. To conduct a direct comparison, I have developed an extended pattern search algorithm, genetic algorithm, particle swarm optimization, and multi-objective genetic algorithm that accept the same cost and wake models, and have comparable optimization settings. Each algorithm explicitly or implicitly enforces constraints that each turbine is within the bounds of the farm and that no turbine is within 200 m of another turbine. The following subsections detail those algorithms.

4.1 Extended Pattern Search

While many heuristic algorithms rely on large populations of possible solutions, the Extended Pattern Search algorithm (EPS) makes continuous improvements to a single solution. It first generates a layout without any constraint violations. The algorithm then randomly cycles through each turbine in the field, attempting prescribed turbine movements. A turbine is moved first in the negative y direction one initial step size. If the objective evaluation of the entire layout improves and no constraints are violated, the

move is kept. Otherwise the turbine returns to its original position and attempts moves at the initial step size in the negative x, positive y, and positive x directions until a move is kept or all directions have been attempted. If the turbine in question is located in the downwind half of the field, the algorithm attempts the search directions in the opposite order, to reduce the likelihood of constraint violations.

When no turbine can accept a move at the initial step size, the EPS begins "popping" poor performing turbines to new locations. The popping algorithm applies sequentially to the 5 worst performing turbines. If the evaluation of the entire field improves and no constraints are violated, the new location is kept and the next turbine is popped. Each turbine is allowed 1000 popping attempts per iteration. If no pops are accepted, the algorithm continues onto the next turbine.

After popping the worst performing turbines, the EPS begins cycling through individual turbines again at one half the original step size. The algorithm terminates when no moves can be found at the minimum step size of 3 m.

Fig. 4.1 gives the pseudocode of the EPS algorithm described in this section.

4.2 Genetic Algorithm

A genetic algorithm is a heuristic optimization method that mimics the passing down of optimal traits through reproduction over many generations. The genetic algorithm (GA) developed for this work requires the wind farm space to be discretized into five meter increments. Turbines may only be placed on the vertices of the mesh. The 5 m mesh size results in 401 options for every turbine's x– and y–location in a 2000 m x 2000 m field. While this mesh size is significantly smaller than that used by most existing GA wind farm optimization formulations, the finer discretization is required for reasonable comparison with the non-discretized EPS.

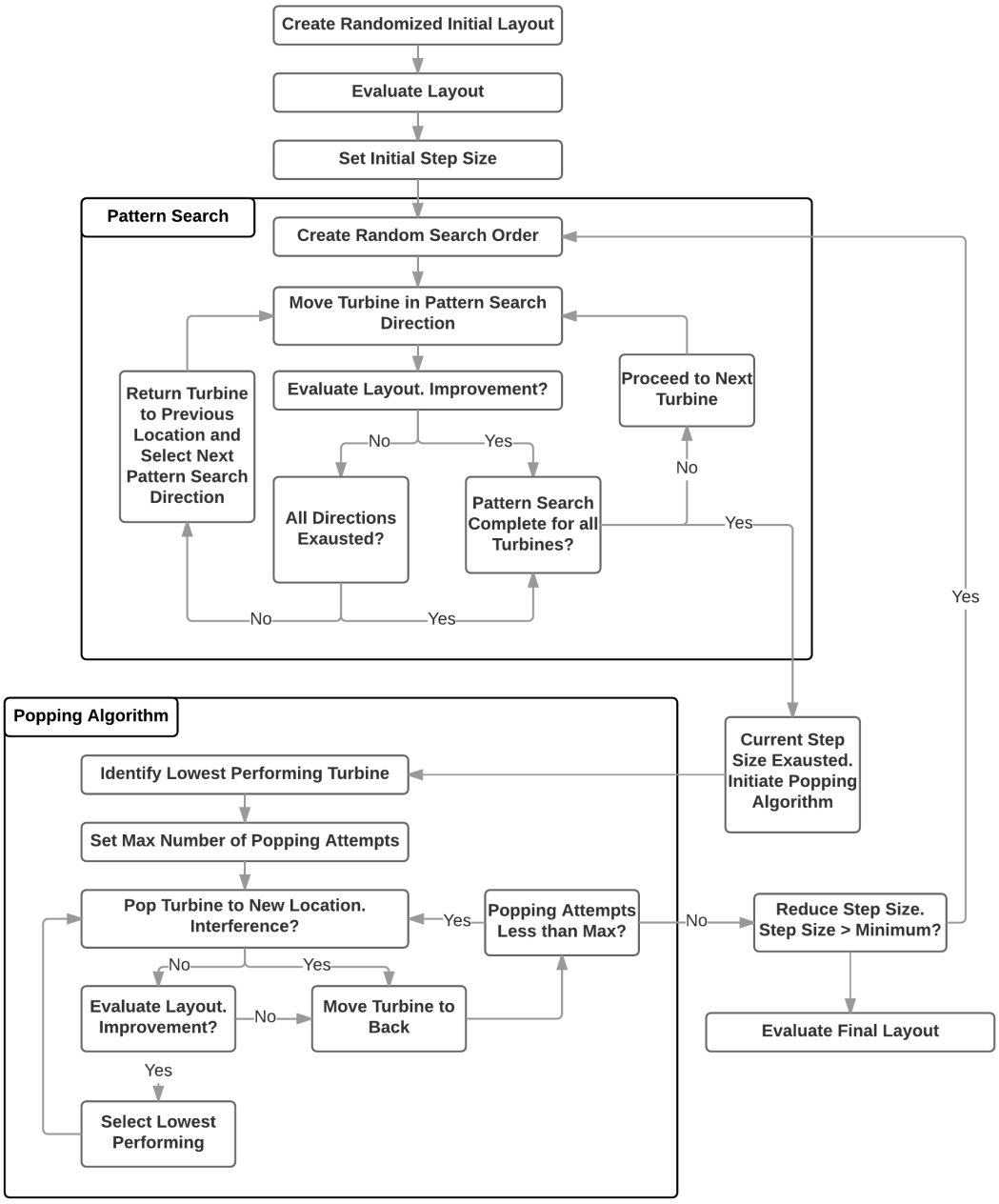

FIGURE 4.1: Pseudocode of EPS Algorithm

A wind farm is represented in the GA as a string of binary values. This string is translated into turbine x– and y–locations using a predetermined algorithm. Through cross-over and random mutation, as described in section 2.4, the GA strategically selects new turbine layouts.

In this genetic algorithm the best scoring 10% of the adult population is copied into the child population and the worst scoring 20% of the adult population are removed before mating. The top scoring 80% of adult layouts are then ordered and mated by score; coupling the best scoring adult with the second best and the third best scoring adult with the fourth until all remaining adults are paired.

Mating is simulated through the crossover of the binary strings representing turbine layouts. The cross-over point is randomly selected, and resulting possible children are added to an empty list. After mating, 5% of the possible children in that list are subjected to a random mutation in a single gene. After crossover and mutation, all children are examined for constraint violations. Only the potential children that do not violate any constraints are added to the child population. The rest of the child population is then filled with randomly generated, non-violating layouts until the predetermined population size of 100 layouts is reached.

The GA convergences after 100 generations without improvement in the population's best objective function. Once the convergence criterion is met, the algorithm returns the best-ranked layout in the child population.

Fig. 4.2 gives the pseudocode of the GA described in this section.

4.3 Particle Swarm Optimization

Particle Swarm Optimization (PSO) is an optimization technique that emulates the swarming behavior of birds and fish to locate optimal solutions. The PSO used in this

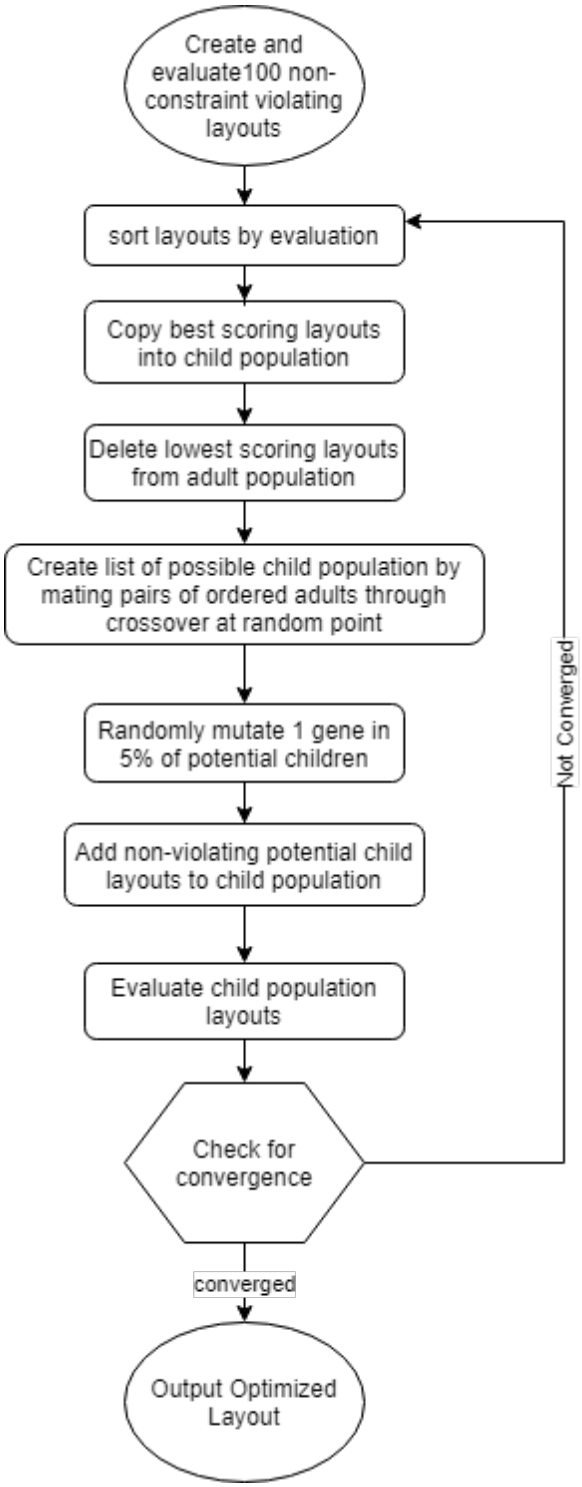

FIGURE 4.2: Pseudocode of Genetic Algorithm

work begins with 100 randomly generated layouts in compliance with all constraints, much like the GA. The initial layout with the lowest objective evaluation is then identified and recorded to preserve the swarm's best layout to date. To begin the optimization process, each layout is assigned a random initial velocity in the x– and y–direction between 0 and 2 m. At every iteration the velocity of individual turbines is updated according to Eq. (4.1).

$$v_{ij,k} = v_{ij,k-1} + C_1 r_1 (d_{ij,k-1} - d_{ij,best}) + C_2 r_2 (d_{ij,k-1} - d_{i,swarmbest}) \tag{4.1}$$

In this function v is turbine velocity, d is current location, i is the individual turbine number, j is the layout number in the swarm, and k is the iteration. $d_{21,best}$ thus indicates the location of turbine 2 in the layout with the lowest objective in the history of layout 1, while $d_{2,swarmbest}$ indicates the location of turbine 2 in the layout with the lowest objective evaluation in the swarm's history. C_1 and C_2 are weightings given to the layout's best and swarm's best performances. In this model $C_1 = C_2 = 0.001$. While a value of 0.001 is very low for a typical PSO, I discovered that limiting the velocity of turbines resulted in better outcomes that did not violate constraints.

Rather than explicitly enforce spacial constraints on the turbines, the PSO uses a penalty factor to discourage layouts that violate constraints. The penalty is added into the objective evaluation given in Eq. (4.2)

$$objective = \frac{Cost_{total}}{Power_{total}}(1 + \sum CV) \tag{4.2}$$

In this function CV is the sum of constraint violations for every turbine in the layout. For turbines outside the 2000 m bounding area, the CV is the shortest distance from the turbine's location to the bounding area. For turbines within 200 m of another turbine, the CV is 200 m minus the distance between the violating turbines in meters.

After each movement, the algorithm updates the best layouts for each layout number and the swarm as a whole. This process continues until 100 iterations have been completed

without an improvement in the swarm's best objective function. The algorithm returns the best layout with the lowest evaluation in the swarm's history.

Fig. 4.3 gives the pseudocode of the PSO described in this section.

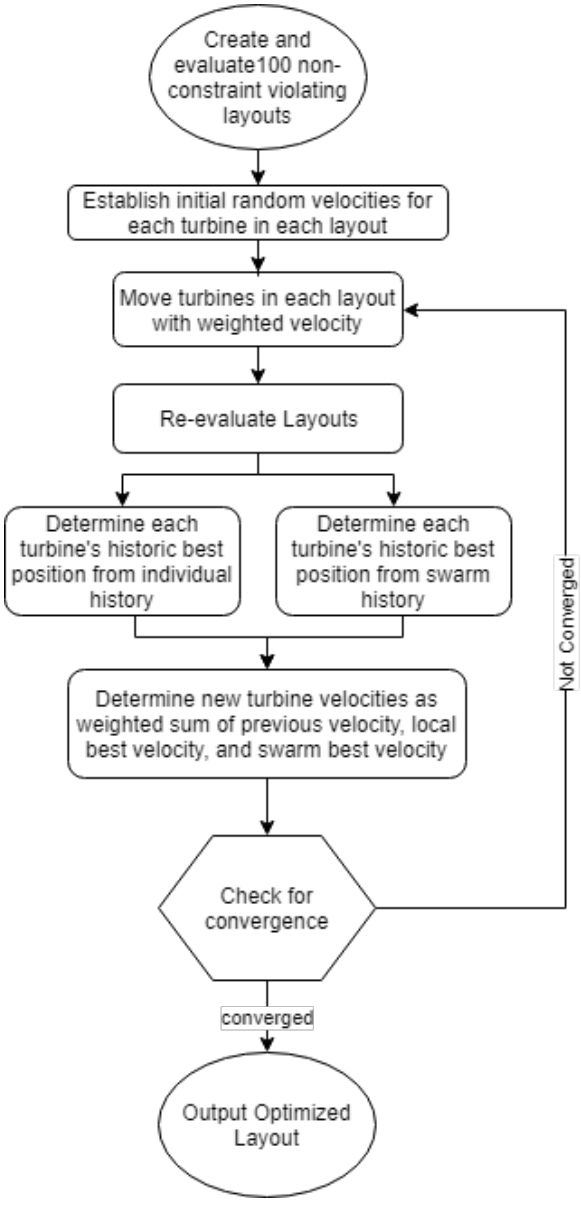

FIGURE 4.3: PSO Pseudocode

4.4 Multi-objective Genetic Algorithm

In this research, single-objective functions consider farm power production and costs. I use the NSGA-II multi-objective optimization algorithm to maximize power production and minimize costs separately [47]. The NSGA-II algorithm estimates points on the Pareto frontier for a farm with 21 turbines, in accordance with the optimal farm found in the single-objective optimization formulation. After each generation, new layouts are added to the pool of possible Pareto points from the previous generation. Each possible Pareto point is then examined for non-dominance, and non-dominated points are retained for use in the next generation. The algorithm terminates when 40 Pareto point approximations are retained.

5 PROBLEM FORMULATION

5.1 Summary of Studies to be Conducted

To address problems in the wind industry involving a need for improved turbine layout optimization and modeling, I have developed the five studies described in this chapter. To determine the most appropriate optimization algorithm for application to the wind farm layout problem, I will compare the functionality of three heuristic algorithms under simplified wind conditions. The selected algorithm from this study is then used to compare the optimization of onshore and offshore wind farms under the same wind conditions, minimizing the cost per unit power and LCOE of wind farms. My third study optimizes offshore wind farms under a more realistic wind case shown in Fig. 8.2.

The final two studies in this report focus on input models to optimization rather than optimization itself. The fourth study compares the accuracy and computational expense of a high-fidelity CFD wake model and a simplified linear wake model. The final study examines turbine availability modeling.

5.2 Algorithm Selection

The purpose of this experiment is to determine the best algorithm for floating offshore wind farm optimization as defined by the quality of the output as well as the algorithm's computational expense. I make this determination by optimizing the locations of 5–30 turbines under unidirectional, constant-speed winds using each of the single-objective optimization techniques described in section 4 Each algorithm is used to minimize the cost per unit power of the farm as a whole. Each turbine has a rotor radius of 40 m and a hub height of 80 m. The optimization is conducted five times with each algorithm and each

input number of turbines to account for algorithmic stochasticity. The environmental parameters for optimization are given in the offshore column of Table 5.1. A Multi-Objective GA (MOGA) is implemented to compare performance against single-objective optimization and explore the trade-off between a farm's power production and its cost.

Additionally, I compare the results of the offshore optimization against the Adapted Genetic Algorithm (AGA) presented by Liu and Wang [28]. To enable this comparison, parameters of the floating offshore wind farm optimization approach were made consistent with the AGA approach — the objective function was changed to maximize the power output of 16 wind turbines in a 4 km by 4 km field under unidirectional, constant wind speeds. The ambient wind speed is taken to be $12\,\mathrm{m\,s^{-1}}$, and the surface roughness is 0.0005 m. The turbines have a rated power of 5 MW and a rated wind speed of $14\,\mathrm{m\,s^{-1}}$. The PARK wake model is applied to determine downstream wind speeds, and the power curve derived by Liu and Wang is used to determine power output [28]. After ensuring that the EPS could return results with the power output and efficiency of Liu and Wang's AGA, the EPS was applied to a continuously larger number of turbines until a 100% efficient layout could no longer be found. In wind farm optimization, efficiency is taken to mean the total power output of a farm divided by the sum of the power output of the individual turbines without wake effects. This study is conducted in Chapter 6.

5.3 Unidirectional Wind Case

The purpose of this study is to understand the differences between onshore and offshore farm optimization by exploring a simplified, consistent unidirectional wind case. In this work I make several assumptions detailed in the following paragraphs. Both onshore and offshore wind farms are square in area with side lengths of two kilometers. The site locations are suitable for wind farms, and there are no constraints on the use of the area.

Turbines have a rotor radius of 40 m and a hub height of 80 m. This simplified wind case was chosen to isolate the behavior of the onshore and offshore cost models used in this work. To be consistent with objectives from relevant literature, this study is conducted twice; first with a cost per unit power objective and then with a levelized cost of energy (LCOE) objective.

Surface roughness of a calm open sea has an empirical value of z_0=0.0005 meters, while the onshore surface roughness has a value of z_0=0.05 meters [41]. The power law exponent, α_h, is equal to 0.11 for most offshore locations and stability conditions, and 0.15567 for onshore conditions under neutral atmospheric conditions [9, 48, 36]. The worst-performing five turbines are popped in the third stochastic extension, and the maximum number of popping attempts is 1000. The wind farm has 20-year lifetime. The water depth of floating offshore farms is 200 meters, and the distance from shore is 16 kilometers. The minimum step size is three meters. The floating offshore and onshore wind farm optimization parameters are given in Table 5.1.

To better understand the impact of the density of turbine placement, the EPS accommodates a user-defined number of turbine agents between 5 and 40. The EPS is run five times for each number of turbines under both onshore and floating offshore conditions using both objective functions. The optimal number of turbines for each farm type is then determined along with the optimal layout of those turbines based on the results of optimization. This study is discussed in Chapter 7.

5.4 Multidirectional Wind Case

To more accurately reflect real conditions, I adapted the EPS algorithm to accommodate multiple wind directions and speeds. The wind regime used in this test case was taken from Grady et al. and is shown in Fig. 8.1 [49]. Degree values in Fig. 8.1 repre-

TABLE 5.1: Environmental Characteristics

Parameter	Onshore Scenario	Offshore Scenario
Side Length	2000 m	2000 m
Water Depth	200 m	200 m
Life of farm	20 years	20 years
Distance from Shore	N/A	16 km
Surface Roughness	0.05 m	0.0005 m
Wind Speed	$10\,\mathrm{m\,s^{-1}}$	$10\,\mathrm{m\,s^{-1}}$
Power Law Exponent	0.15567	0.11
Number of Popping Attempts	1000	1000
Number of Popped Turbines	5	5
Turbine Cut-in Speed	$3\,\mathrm{m\,s^{-1}}$	$3\,\mathrm{m\,s^{-1}}$
Turbine Rated Speed	$11.5\,\mathrm{m\,s^{-1}}$	$11.5\,\mathrm{m\,s^{-1}}$

sent clockwise directional deviation with zero degrees indicating wind originating from the bottom of the field (positive y direction). The case study also included five optimization trials for each farm size from 5–40 turbines. As with the unidirectional case, results are presented for the minimization of cost per unit power as well as LCOE. Results from this study are presented in chapter 8.

5.5 Wake Model Selection

The level of fidelity in wake models for wind farms is closely tied to and positively correlated with computational expense. There is a research gap in understanding and quan-

tifying the trade-offs between high fidelity CFD wind field analysis and simplified linear wake models. The goal of this section is to identify relative performance patterns between CFD and linearized wake models and determine where the higher-expense CFD analysis is justified through increases in accuracy. This analysis compares NREL's WindSE2D software to a 2D implementation of the PARK wake model by analyzing wind speeds throughout an onshore wind farm. The analysis is broken into two sections comparing 1) the relative response of wake models to hard coded layouts and 2) the absolute accuracy of each model using real wind data.

5.5.1 Relative Response of Wake Models

In this case I analyze several hard-coded layouts beginning with placing two and three turbines respectively at equal down-wind spacing and comparing the resulting percent difference in power development. This turbine setup is depicted in Fig. 9.1. These tests were conducted using optimal power conditions ($C_p = 16/27$, $a = 1/3$, $C_t = 8/9$) as well as a more realistic scenario with $C_p = 0.34$, $a = 0.25$, $C_t = 0.75$. The realistic wind case used was taken from King et al. [24].

After the two– and three–turbine tests, I analyzed four hard coded layouts using the CFD wake model and the Jensen model with and without a nested wake provision to better account for multiple nested wakes. These layouts are shown in Fig. 9.2. The "optimized" layout was generated from an extended pattern search using the Jensen wake model in a previous work.

5.5.2 Absolute Accuracy Analysis for Wake Models

After examining relative performance of each wake model, I used 3,612 data points from a select field of a wind farm in Colorado to determine the absolute accuracy of each wake model. Fig. 9.3 shows the layout of this select field and Fig. 9.4 gives wind onset angles, speeds, and probabilities describing the input data. In Fig. 9.4, 270^o indicates wind

originating from the left side of Fig. 9.3. Larger onset angles indicate clockwise variation of wind origin.

For each data point, I used the ambient wind speed and wind onset angle from the on-site meteorological tower, depicted as a diamond in Fig 9.3, to calculate the wind speed at each turbine using each wake model. Average and root mean square errors were then calculated to compare modeled turbine wind speed to wind speed readings from each turbine's nacelle anemometer. This experiment is conducted using the WindSE2D wake model as well as 2 variations of the Jensen wake model, one in its original form, and another with an added nested wake provision to improve model accuracy. Results and conclusions from this study may be found in chapter 9.

5.6 Turbine Availability Modeling

Producible energy refers to the energy that could be produced by a wind turbine, given the turbine's operating specifications and local atmospheric conditions. Period energy is the producible energy, minus losses due to forces outside the turbine operator or manufacturer's control, such as curtailments, ice on blades, ambient temperatures outside the turbine operating range, and extreme weather events such as hurricanes and tornadoes. Energetic availability is the percentage of period energy that a wind turbine actually captures, and it reflects turbine downtime as a result of forces within the turbine operator or manufacturer's control.

5.6.1 Availability by Manufacturer as a Function of Environmental Factors

To identify the primary factors governing wind turbine energetic availability I conducted a statistical exploration of availability binned by external and internal factors of interest including time of day, season, average wind speed, ambient temperature, frequency of curtailment, age of farm, and turbine alarm readings. In this study, we employed data

sampled every five minutes for 38 US-based onshore wind assets ranging from January 2013 to December 2016.

5.6.2 Avoidable Losses as a Function of Turbine Manufacturer

Results from the availability analysis formulated in Section 5.6.1 showed distinct variations in turbine availability between manufacturers. To understand the root of these variations, I first created time series plots for each manufacturer of the percentage of cumulative producible energy that was lost due to malfunctions in the turbine, electrical grid, and substation. I then narrowed my scope to turbine-specific outages and examined the top 65% of outages as measured by lost generation. I examined alarms triggered during each of these turbine stoppages and developed an algorithm to attribute an alarm of cause. After identifying the alarm of cause, and thus the malfunctioning turbine component, I grouped turbine losses into larger functional areas (eg., gearbox, generator, pitch system), and plotted losses attributed to those functional areas for each manufacturer. This study is conducted in chapter 10.

6 ALGORITHM SELECTION RESULTS AND DISCUSSION

6.1 Algorithm Selection Results

Internal Algorithm Comparison

The results of of floating offshore wind farm optimization using the four identified algorithms are discussed in this chapter. Fig. 6.1 shows the final objective evaluation from each single-objective algorithm against the number of turbines optimized and fits a fifth-degree polynomial for each algorithm. The number of objective evaluations and time taken for each trial are shown in Fig. 6.2a and 6.2b respectively. The lowest-objective layout found by each optimization algorithm is summarized in Table 6.1. The EPS returned the lowest-objective evaluation of the three algorithms, and returned a farm with more turbines than the optimized farms from the other algorithms. This layout is shown in Fig. 6.3, where blue triangles represent turbines and dashed lines represent the boundary of turbine wakes.

Fig. 6.4a shows an estimated Pareto frontier resulting from the multi-objective genetic algorithm which maximizes power production while minimizing farm costs. The figure is replicated in Fig. 6.4b with the addition of the point representing the best single objective optimization using the EPS in red.

TABLE 6.1: Comparative Optimization Results

Optimization Technique	Number of Turbines	Objective ($\$kW^{-1}$)
Genetic Algorithm	19	20,366
Particle Swarm Optimization	13	21,434
Extended Pattern Search	21	20,146

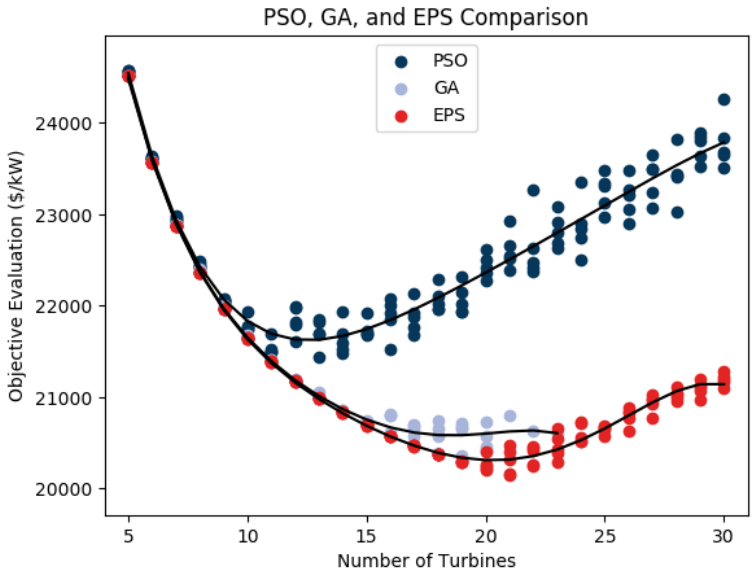

FIGURE 6.1: Results of Optimization with each Algorithm

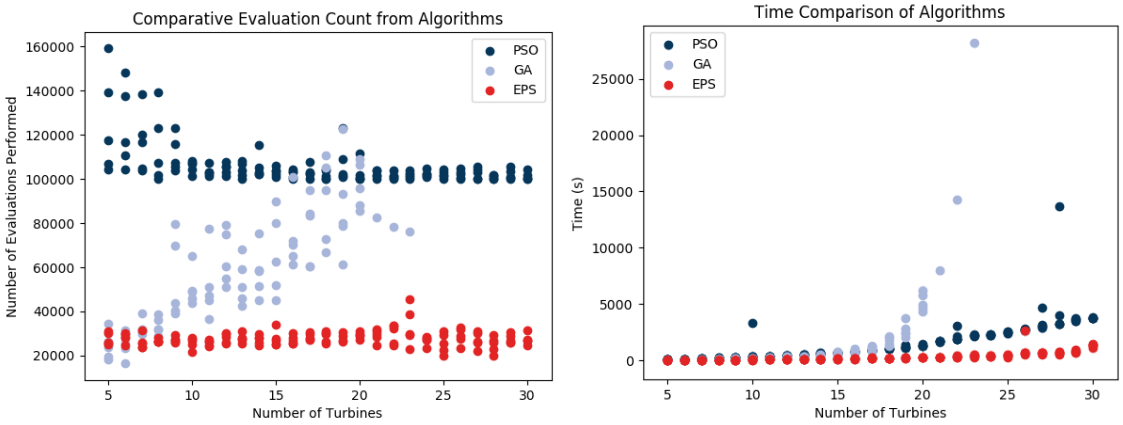

(a) Evaluations to Optimization

(b) Time to Optimization

FIGURE 6.2: Algorithmic Expense Comparison

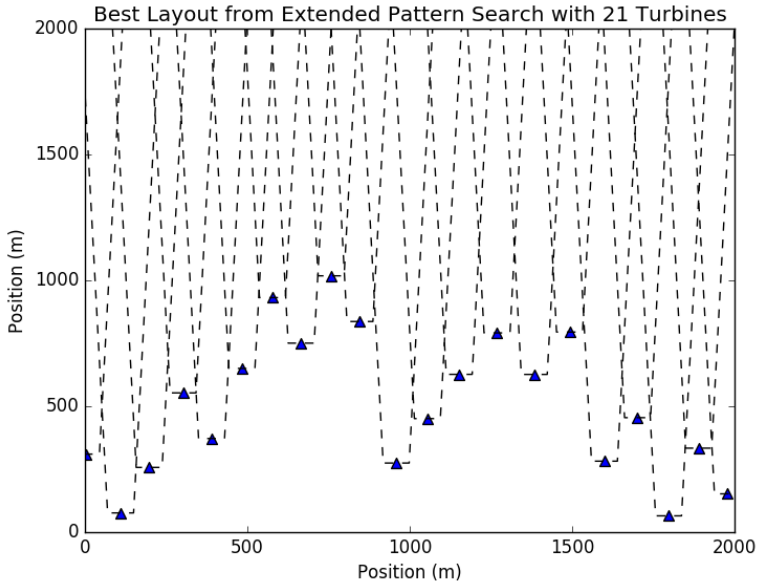

FIGURE 6.3: Overall Lowest Objective Layout

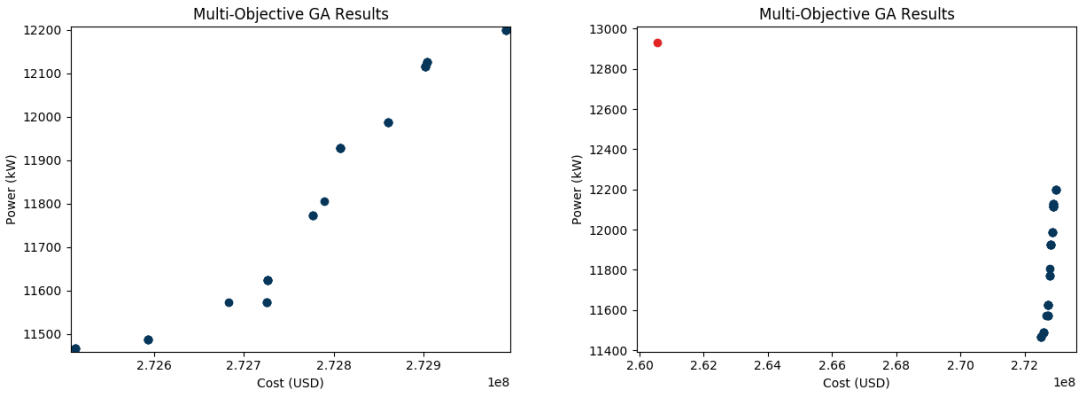

(a) Multi-objective optimization results (b) Results with optimized single objective (red)

FIGURE 6.4: Multi-Objective Optimization Results

EPS Comparison to Existing Study

Liu an Wang used a Adapted Genetic Algorithm to optimize the placement of 16 offshore turbines in a 4 km by 4 km field. The algorithm maximized the annual energy production of these turbines. Using this objective, any layout that can achieve 100% efficiency constitutes a global optimum.

There are numerous turbine layouts that result in 100% efficiency (no reduction in power output due to turbine wake effects) for 16 turbines in a 4 km by 4 km field. The EPS used in this study should consequently be able to find a 100% efficient layout each trial. The EPS was able to find a 100% efficient layout for each of 10 trials performed, thus further validating the capability of the EPS.

After finding multiple 100% efficient 16-turbine layouts, the EPS was applied to increasingly large numbers of turbines in the 4 km by 4 km space. The algorithm was able to find a 100% efficient layout for farms containing up to 34 turbines. One such 34 turbine layout is shown in Fig. 6.5.

6.2 Algorithm Selection Discussion

Algorithm Comparison

Fig. 6.1 shows that the PSO resulted in worse layouts with fewer turbines than the GA or EPS. This is most likely due to the inability of the PSO to explicitly handle the constraints given in the problem. The penalty function used in the PSO applied to the objective of the entire field, and may have been improved by targeting poorly behaving turbines.

Both the GA and the EPS provided similarly optimal layouts, with the EPS showing only slight improvement over the GA. Since both of these algorithms performed well, I selected the algorithm that best balanced optimization effectiveness and computational

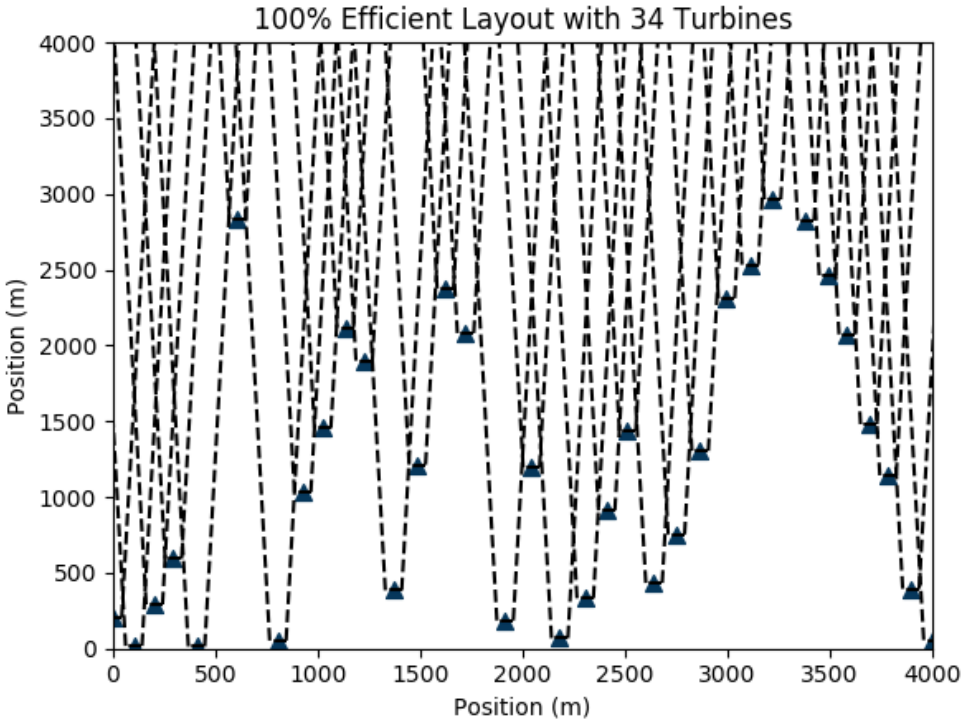

FIGURE 6.5: 100% Efficient 34 Turbine Layout [3]

expense. The number of function evaluations required for optimization by all three algorithms is given as a function of the number of turbines being optimized in Fig. 6.2a. The total time required to perform optimization is a function of the memory necessary, as well as the number of function evaluations required and consequently displays different patterns across algorithms than the number of evaluations. Time information is recorded in Fig. 6.2b. The time expenditure of the GA starts to increase exponentially around 20 turbines, while the EPS takes a similar amount of time to run regardless of the number of turbines being optimized. The EPS runs more quickly than the GA because it requires far less computer memory and fewer objective evaluations for larger fields. The GA's representation of each turbine in a farm uses significantly more memory than that of the EPS and PSO. The EPS may run more quickly because it improves a single layout instead of generating hundreds of new layouts like the GA or PSO.

The results of this work suggest that an EPS is superior to a PSO or GA when it comes to optimizing floating offshore wind farm layouts in a unidirectional constant wind speed scenario, especially when considering larger wind farms. While the computational expense of the GA resulted in fewer experimental data points, Fig. 6.1 alludes to superior optimization performance by the EPS.

The multi-objective GA explores the idea of maximizing power output while minimizing cost. While the single objective algorithms perform a similar task through the use of an objective function considering both goals, the multi-objective optimization provides an array of non-dominated and thus "ideal" solutions. In theory, the optimal point found by the single objective optimizations would be on the Pareto frontier developed by the multi-objective genetic algorithm. The optimized single-objectibe solution, designated by the red point in Fig. 6.4b, dominates several of the solutions on the Pareto frontier. The results from this optimization indicate that a multi-objective genetic algorithm may not perform as well as single objective optimization studies.

EPS Comparison to Existing Study

Both the Adapted GA from Liu and Wang and the EPS in this work were able to find 100% efficient layouts for 16 turbines on a 4 km by 4 km farm. With only a 200 m separation constraint between turbines, there is a large solution space (a large number of different turbine layouts) resulting in 100% farm efficiency. As the number of turbines was increased, it became more difficult to find a 100% efficient layout. Liu and Wang did not provide data for the optimization of more than 16 turbines, so the algorithms cannot be compared in terms of the maximum number of 100% efficient turbines on the farm [28]. However, the continuous solution space allowed by the EPS indicates a possible advantage over the discretized space used in the Adapted GA. This advantage is consistent with findings from DuPont and Cagan [37].

7 UNIDIRECTIONAL WIND CASE RESULTS AND DISCUSSION

The unidirectional test case, though simplistic, provides a mechanism for understanding the impact of the cost model on optimization. The results of the unidirectional study are presented in the next subsection.

7.1 Unidirectional Wind Case Results

Layouts were optimized using the EPS for wind farms containing 5 to 40 turbines; these turbines each had a hub height of 80 m and a rotor radius of 40 m. The objective evaluation for each layout is plotted against the number of turbines for onshore optimization in Fig 7.1 and floating offshore optimization in Fig. 7.2. Furthermore, a comparison of the optimal layout in terms of raw data and 5th degree polynomial fit are given in Table 7.1. The raw data from the cost per unit power objective suggests an optimal onshore layout with five turbines and an objective evaluation of $\$16.385\,\mathrm{kW}^{-1}$. The polynomial fitting with an R^2 value of 0.9886 suggests an optimal onshore layout with 13 turbines. The onshore layout with the lowest cost per unit power objective is shown in Fig. 7.3, where dashed lines indicate areas impacted by turbine wakes. Fig. 7.1 shows that there is minimal change in the onshore objective evaluation from 5 to 18 turbines, correlating with the range in which the EPS can find 100% efficient layouts. This trend is consistent between both objectives. The best performing 18 turbine layout had a cost per unit power of $\$16.385\,\mathrm{kW}^{-1}$ and an LCOE of \$0.108 . This layout is presented in Fig. 7.4. The best 18 turbine onshore evaluation returned by the EPS is negligibly larger (less optimal) than the best evaluation using 5 turbines for both objectives.

The most optimal floating offshore layout found using the EPS approach includes 21 turbines and had a cost per unit power of \$20.400/(kW h). The optimization using

the LCOE objective also returned an optimal layout of 21 turbines with an evaluation of \$0.141/kWh. A fifth degree polynomial fit to the cost per unit power plot, with an R^2 value of 0.9860, suggested that the optimal number of turbines was 19. The lowest objective offshore layout from the cost per unit power objective is shown in Fig. 7.5.

TABLE 7.1: Optimization results for unidirectional wind case

	Onshore Results		Offshore Results	
	Raw Data	Polynomial Fit	Raw Data	Polynomial Fit
Lowest Cost per Unit Power	$\$16\,362\,\mathrm{kW}^{-1}$	$\$16\,385\,\mathrm{kW}^{-1}$	$\$20\,400\,\mathrm{kW}^{-1}$	$\$20\,543\,\mathrm{kW}^{-1}$
Number of Turbines	5	13	21	19
R^2 Value	-	0.9886	-	0.9860
Lowest LCOE	\$0.108/(kW h)	\$0.108/(kW h)	\$0.141/(kW h)	\$0.142/kWh
Number of Turbines	5	12	21	26
R^2 Value	-	0.9892	-	0.9970

7.2 Unidirectional Wind Case Discussion

The deviation in the optimal number of turbines for the onshore and floating offshore unidirectional wind case can be attributed to differences in two primary factors: cost and surface roughness. The surface roughness for both onshore and floating offshore environments are given in Table 5.1. The surface roughness value affects the shape of a wake behind a rotor, with the larger onshore surface roughness resulting in wider wakes, which encompass a greater area, but which regain wind speed more quickly with downstream distance.

In the unidirectional wind case, two identical turbines operating according to the

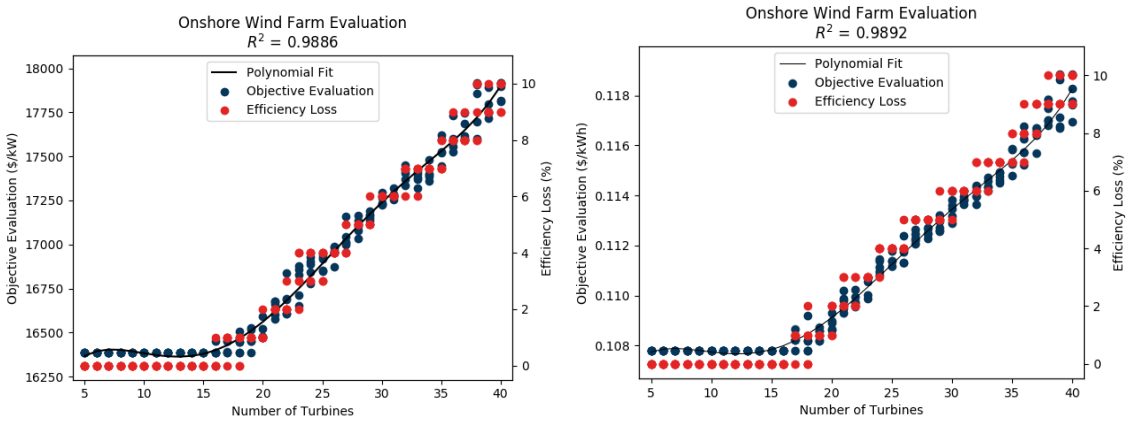

(a) Cost per Unit Power (b) LCOE

FIGURE 7.1: Onshore turbine layout optimization under unidirectional wind case[3]

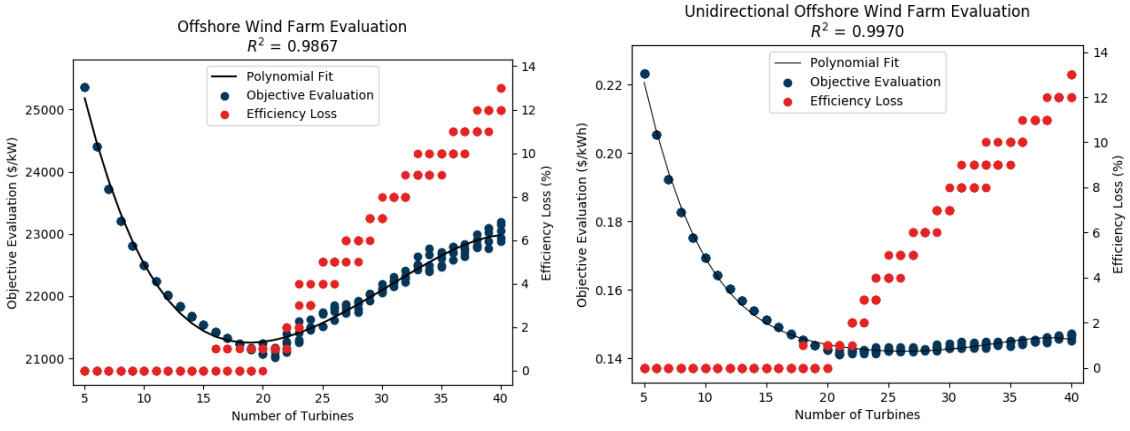

(a) Cost per Unit Power (b) LCOE

FIGURE 7.2: Offshore turbine layout optimization under unidirectional wind case [3]

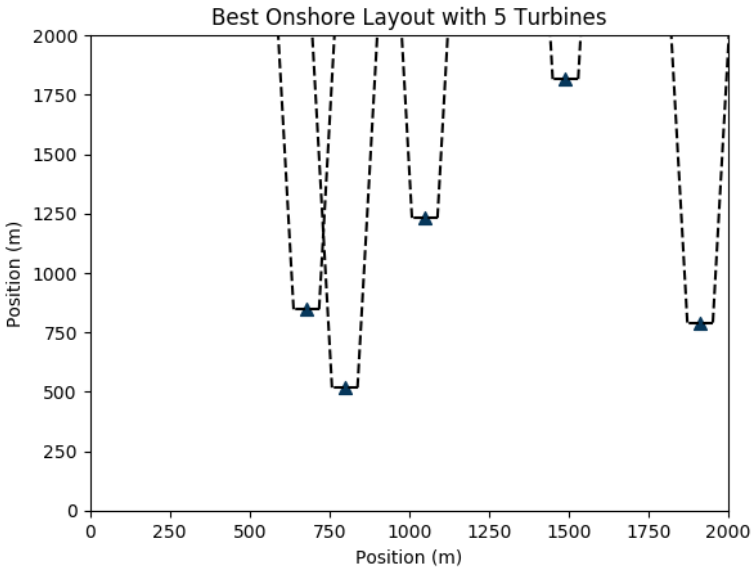

FIGURE 7.3: Best onshore layout under unidirectional, constant wind

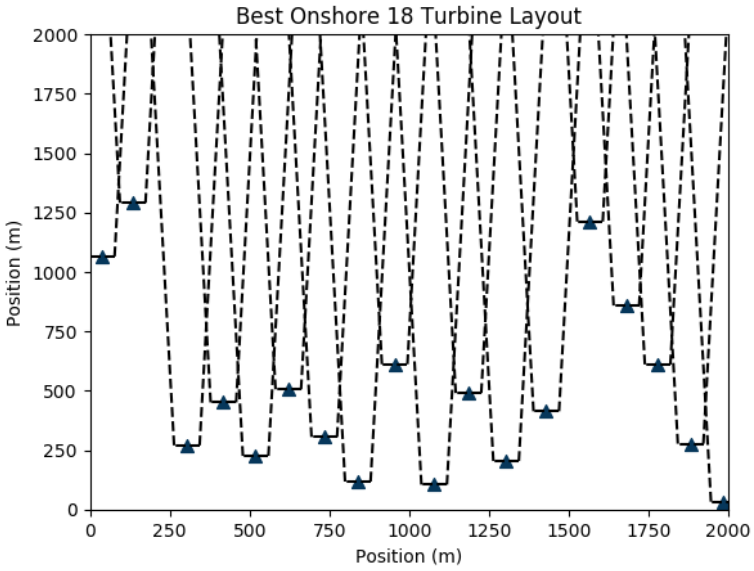

FIGURE 7.4: 18 Turbine onshore layout under unidirectional, constant wind

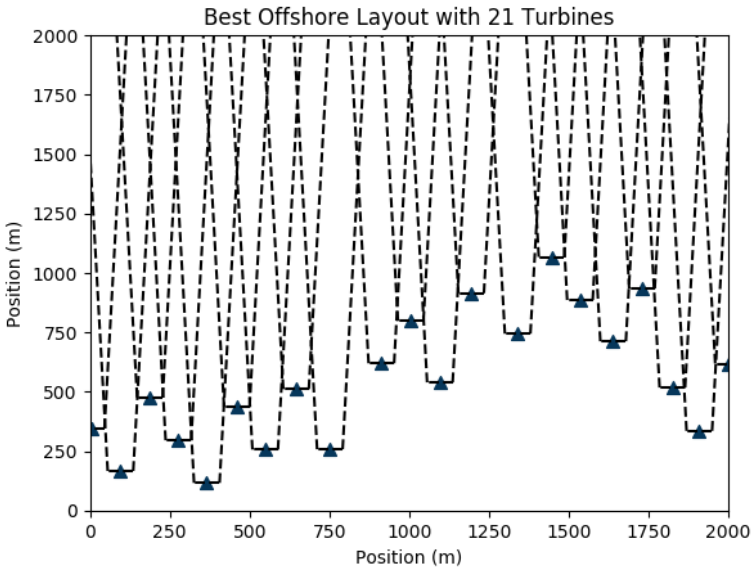

FIGURE 7.5: Best offshore layout under unidirectional, constant wind

floating offshore cost model presented would contribute equally to the cost of a wind farm. However, a turbine in the wake of a second turbine would generate less power than a turbine in unobstructed wind conditions. With a cost per unit power objective, a turbine within another turbine's wake would decrease the possible produced power but leave cost unchanged. This effect led the EPS to favor turbine layouts with minimal wake interference. This finding is intuitive, and is also consistent with previous unidirectional research findings. As shown in Fig. 7.2, the objective function decreased in the floating offshore case until a 100% efficient layout could no longer be found. For layouts with more turbines, the cost per unit power begins to increase.

Similarly, the cost per unit power remains constant (with respect to number of turbines) in the onshore case until a 100% efficient layout can no longer be found. The constant objective evaluation at smaller farm sizes is a result of the mechanics of the onshore cost function. Because I use a single turbine size, each additional 100% efficient turbine has no effect on the ratio of cost to energy produced (each turbine contributes an equal cost and an equal quantity of energy). Farms with a high number of turbines and

cannot be optimized for 100% efficiency cause the objective evaluation to increase because the additional turbines contribute the same cost to the farm but produce less energy due to wake effects. This phenomenon indicates that the additional energy produced by adding a turbine would not compensate for the increased farm cost associated with that turbine. The resulting layouts of the optimization of onshore wind systems had fewer wind turbines than the offshore case which may be attributed in part to the impact of the higher surface roughness values on the shape of turbine wakes, as previously discussed.

The offshore layout in Fig. 7.5 shows most turbines are placed such that the tip of the rotor is just outside the wake of an upstream turbine but as close to the enforced 200 m minimum separation distance as possible. This arrangement decreases wake interference thus maximizing power output, while decreased cabling costs minimizes total costs. The results of the optimal floating offshore layout align with expectations. By efficiently packing turbines such that wake interactions between turbines are minimized, energy output is maximized. By placing turbines close together, cost is minimized. The simultaneous minimization of cost and maximization of energy production leads logically to the lowest cost per unit power.

The onshore layout in Fig. 7.3 is more dispersed. This is likely due to the combination of differences in wake shape and cost function mechanics. With a single turbine size, every onshore wind turbine is modeled with the same cost and maximum energy output. Including a model of this type in the objective function results in the same cost per unit power for any 100% efficient layout regardless of the number of turbines being optimized. The 18-turbine onshore layout shows the same condensed placement of turbines just outside of upstream wakes, as seen in the optimized floating floating offshore layout. Differences between the 18-turbine onshore layout and the 21-turbine floating offshore layout may be attributed to respective surface roughness values. The onshore case has a much higher surface roughness than the floating offshore case. A larger surface roughness value results

in larger diameter wakes, allowing for fewer turbines to be placed with 100% efficiency.

The noise in the data for both the onshore and floating offshore objective evaluations is due to the stochasticity of the EPS (Fig. 7.1 and 7.2). Stochastic extensions help to avoid settling on poor-performing local optima; however, factors such as poor initial layouts or insufficient popping attempts can lead to variation in the objective evaluation for layouts containing the same number of turbines. Running these simulations multiple times allowed me to determine when the algorithm was returning poor results and to select better optimized layouts.

8 MULTIDIRECTIONAL WIND CASE RESULTS AND DISCUSSION

Wind speeds and onset angles used in the multidirectional wind case optimization are given in Fig. 8.1.

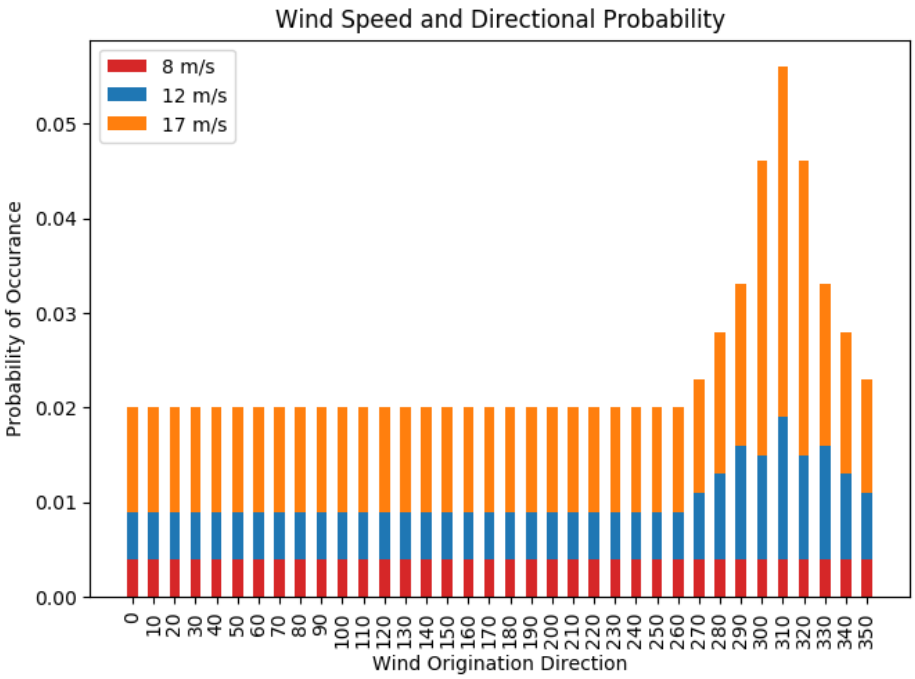

FIGURE 8.1: Wind onset angles and frequency of occurrence for multi-directional wind case [4]

8.1 Multidirectional Wind Case Results

Results from the multidirectional wind case are presented in Table 8.1. Under the multidirectional wind scenario, the most optimal floating offshore layout found using the EPS approach includes 40 turbines and has a cost per unit power of $\$14\,821\,\mathrm{kW}^{-1}$. Using

the LCOE objective, the optimal layout also contained 40 turbines and had an objective evaluation of \$0.099/kWh. A fifth degree polynomial fit using the cost per unit power objective, with an R^2 value of 0.997, suggested that the optimal number of turbines was 40; this was also the highest number of turbines tested. These results are shown in Fig. 8.2. The lowest cost per unit power objective offshore layout is shown in Fig. 8.3. Fig. 8.4 shows a 21 turbine optimized layout to understand the patterns in optimization without the increased turbine packing resulting from wind speeds in excess of the turbine rated wind speed. The 21 turbine layout was selected to be consistent with the optimal number of turbines from the unidirectional wind condition, and is optimized for cost per unit power.

TABLE 8.1: Optimization results for multidirectional wind case

	Raw Data	Polynomial Fit
Lowest Cost per Unit Power	$\$14\,821\,\mathrm{kW}^{-1}$	$\$14\,820\,\mathrm{kW}^{-1}$
Number of Turbines	40	40
R^2 Value	-	0.9970
Lowest LCOE	$\$0.099/(\mathrm{kW\,h})$	$\$0.098/(\mathrm{kW\,h})$
Number of Turbines	40	40
R^2 Value	-	0.9989

8.2 Multidirectional Wind Case Discussion

From the results of the multidirectional wind case, the objective evaluation decreased with increasing farm size until turbines could no longer be placed outside of wakes, at which point the decreases in the objective became smaller with additional turbines. Some wake

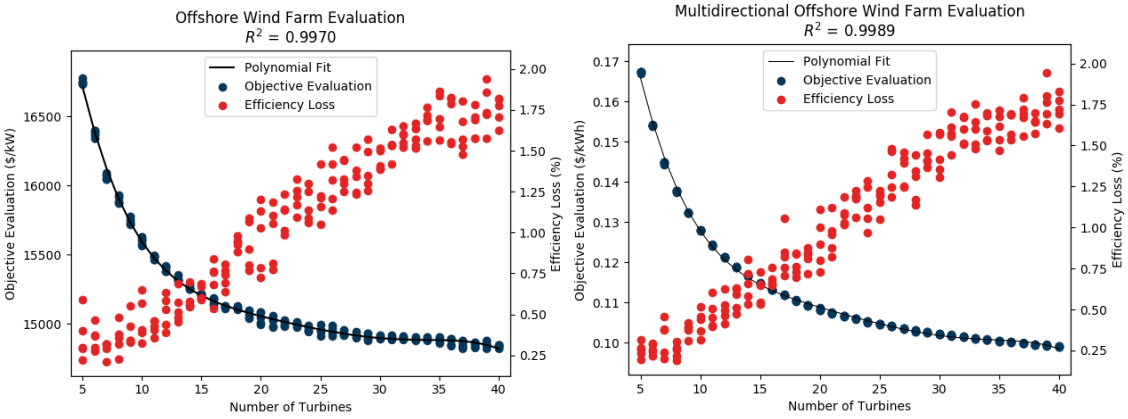

(a) Cost per Unit Power (b) LCOE

FIGURE 8.2: Offshore turbine layout optimization under multidirectional wind case

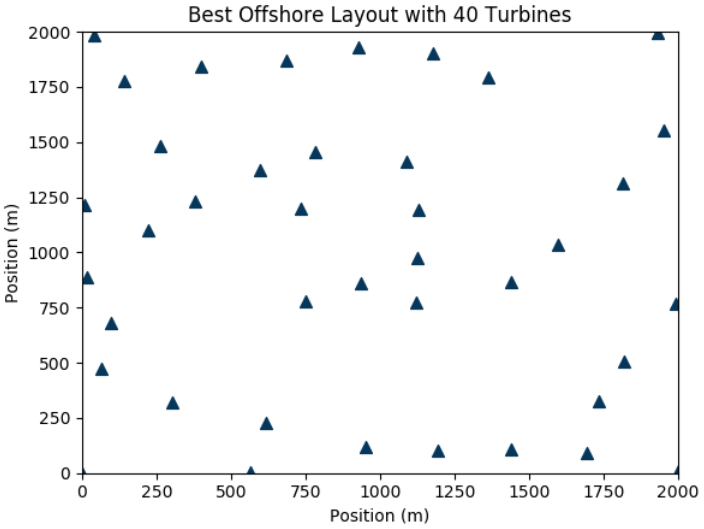

FIGURE 8.3: Offshore turbine layout optimization under multidirectional wind case

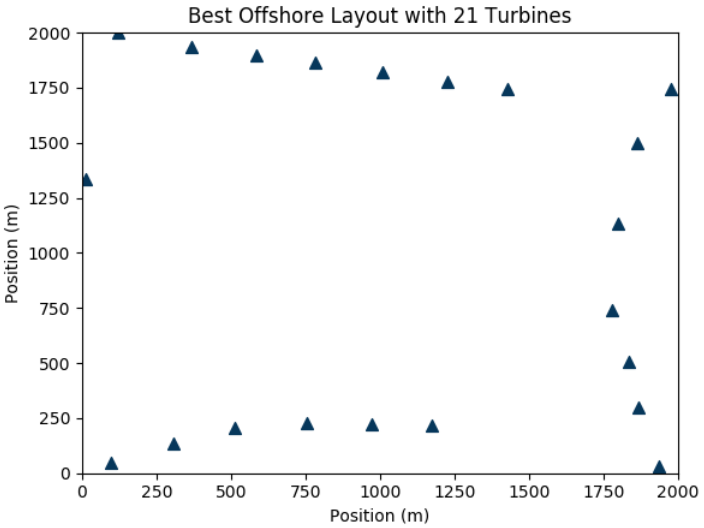

FIGURE 8.4: Offshore optimized 21-turbine layout under multidirectionl wind case

interference between turbines still allowed for 100% efficient layouts at wind speeds in excess of the turbine rated wind speed, meaning that wake effects on downstream turbines left wind speeds in excess of the turbine's rated wind speed. The EPS took advantage of these conditions by packing the field with more turbines. This effect is manifested in the rightward shift of the objective evaluation curve when compared to the unidirectional case. I include an optimized 21-turbine layout to better understand patterns in optimized layouts at lower wind speeds. In this layout turbines move to the edges of the field. This turbine movement decreases wake interference and subsequent power losses, thus resulting in logically better objective evaluations.

The increased wind speeds in the multidirectional case allowed for a closer examination of the relationship between the objective evaluation and wake losses. Results indicated that turbines placed in wakes causing up to 2% farm-wide efficiency losses could still be optimal from a cost per unit power and LCOE perspective. This result indicates that marginal efficiency losses in the multidirectional case could be offset by relatively larger marginal increases in power production. The multidirectional case results allow for slightly

more efficiency loss than the unidirectional case in the optimized solution, but the small efficiency losses are comparable.

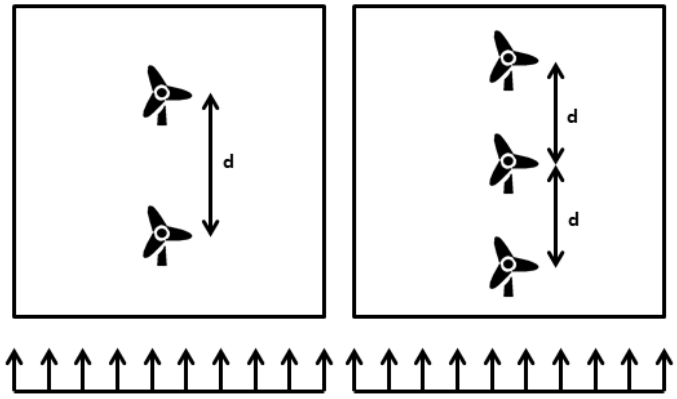

(a) 2 Turbine Layout (b) 3 Turbine Layout

FIGURE 9.1: Inline Turbine Layouts for Wake Model Testing

9 WAKE MODEL SELECTION RESULTS AND DISCUSSION

This study begins with an analysis of two and three inline turbines at equal downwind spacing. These turbine layouts are depicted in Fig. 9.1. Characteristics for the "ideal" and "realistic" conditions under which each layout is analyzed are given in Table 9.1.

TABLE 9.1: Power Conditions for 2- and 3-Turbine Tests

Condition	**Power Coefficient**	**Thrust Coefficient**	**Axial Induction Factor**
Ideal	16/27	8/9	1/3
Realistic	0.34	0.75	0.25

Hard-coded layouts analyzed in section 9.1.1 are depicted in Fig. 9.2.

The turbine layout of the farm used in section 9.1.2 is given in Fig. 9.3. The wind speeds, onset angles, and probabilities of occurrence are shown in Fig. 9.4.

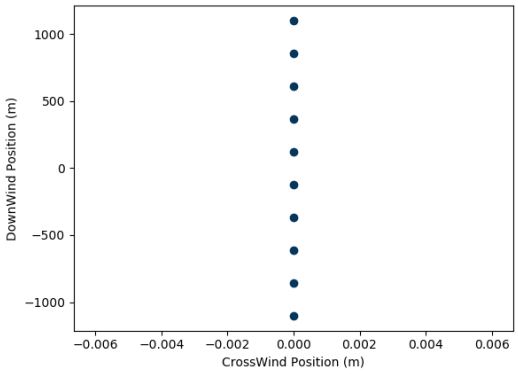

(a) Linear Layout

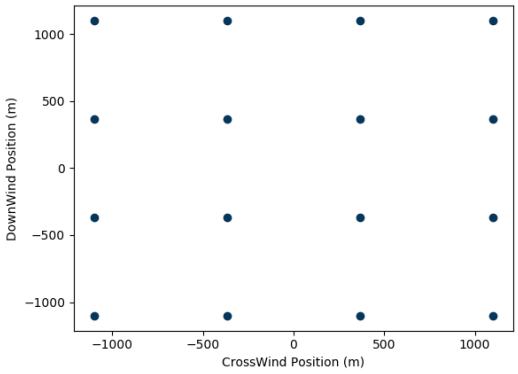

(b) Grid Layout

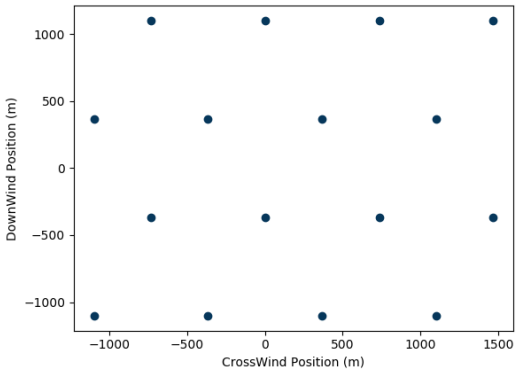

(c) Off Grid Layout

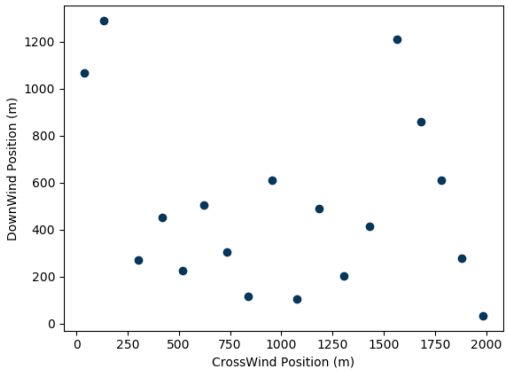

(d) Optimized Layout

FIGURE 9.2: Hard-Coded Layouts for Wake Model Testing

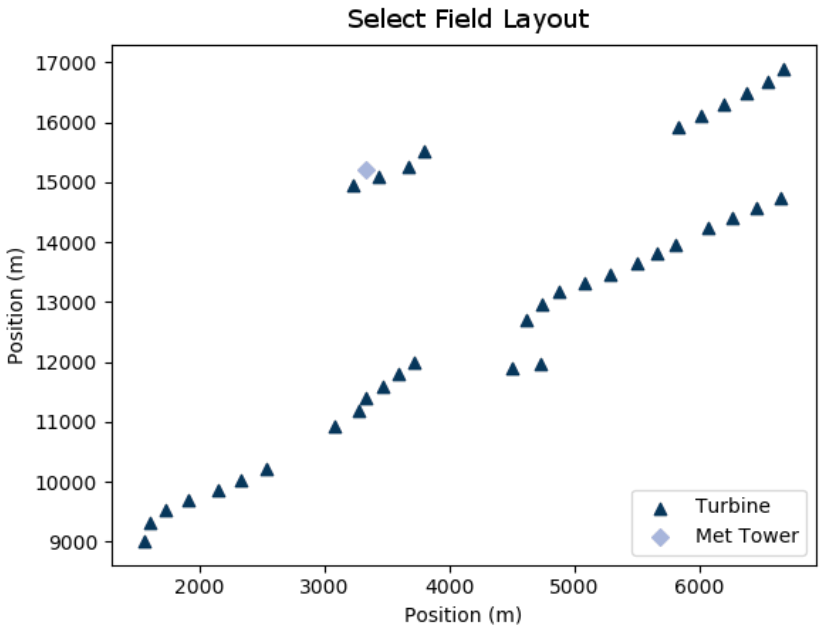

FIGURE 9.3: Select Field Turbine Layout

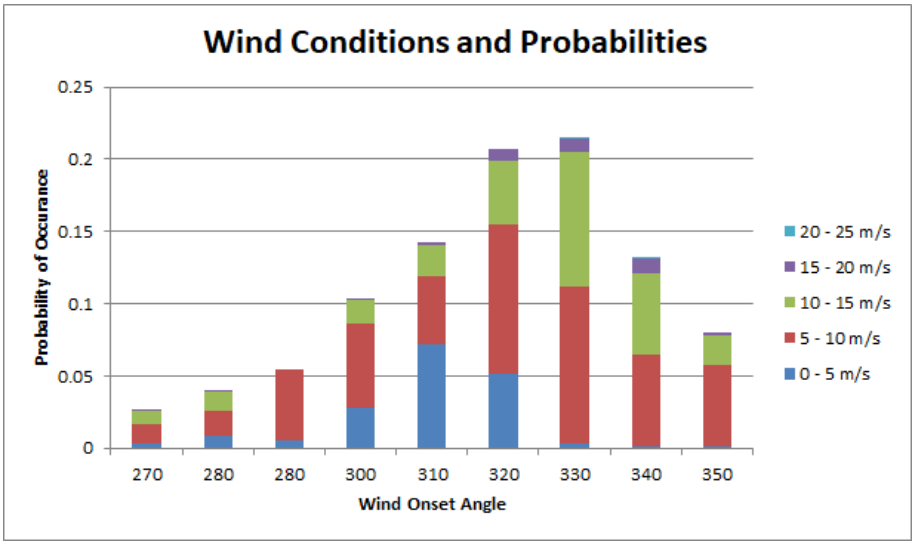

FIGURE 9.4: Wind Conditions and Probabilities

9.1 Wake Model Selection Results

9.1.1 Relative Response of Wake Models Results

The results of testing two inline, downstream turbines with each wake model and power condition are given in Fig. 9.5. The three-turbine test results are shown in Fig. 9.6

under optimal power conditions and Fig.9.7 under sub-optimal power conditions.

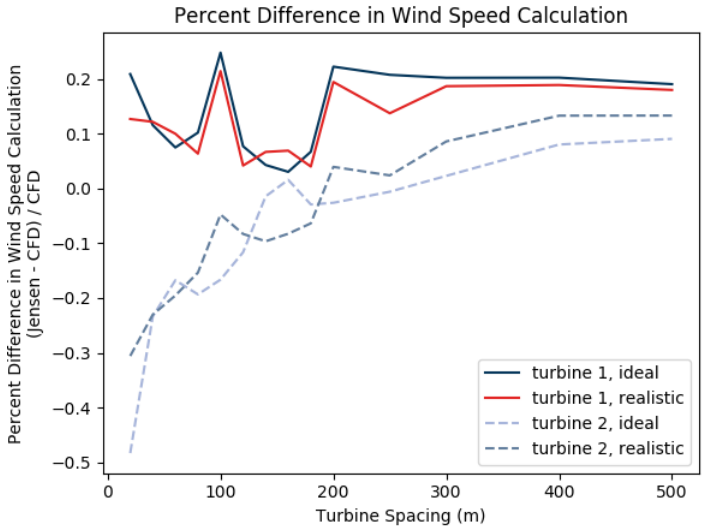

FIGURE 9.5: Percent difference in power development by turbine for two-turbine spacing test

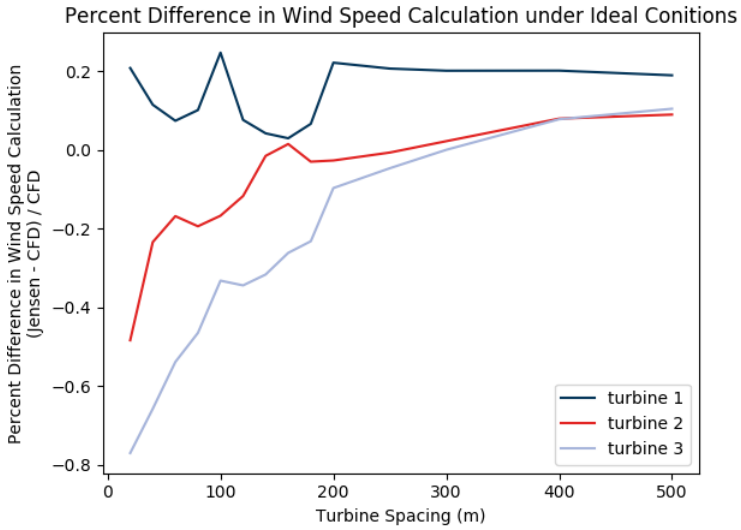

FIGURE 9.6: Three inline turbine power development comparison under optimal power conditions

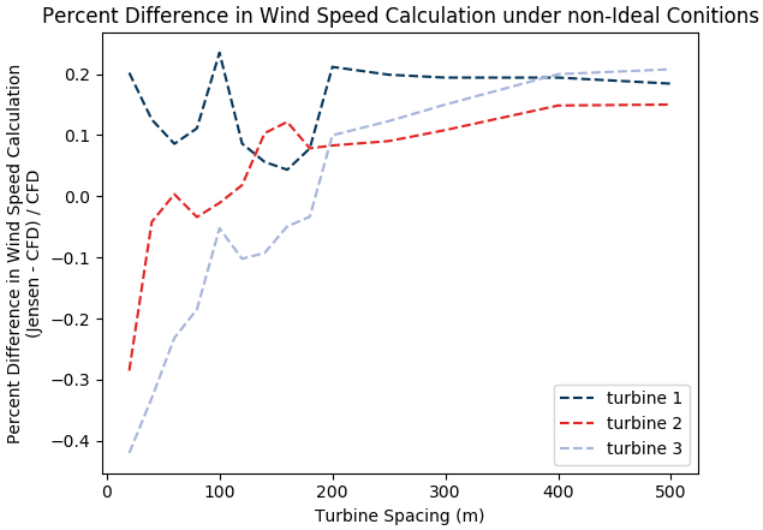

FIGURE 9.7: Three inline turbine power development comparison under sub-optimal power conditions

The results of the hard coded tests are presented in Table 9.2. The nested wake provision allows for closer alignment between the Jensen and CFD wake model for small quantities of nested wakes.

TABLE 9.2: Power Development of Hard Coded Layouts

Modeled Power Development from Hard Coded Layouts				
Model	***16 standard grid***	***16 offset grid***	***10 inline***	***18 Previously optimized***
CFD	7636.734	13067.26	1545.312	16526.39
Jensen	9277.3	13088.27	1831.654	16814.14
Jensen with nested wake provision (NWP)	7256.157	13088.27	1185.179	16814.14
(CFD-Jensen)/CFD	-21.48%	-0.16%	-18.53%	-1.74%
(CFD-Jensen with NWP)/CFD	4.98%	-0.16%	23.30%	-1.74%

9.1.2 Absolute Accuracy Analysis for Wake Models Results

Un-binned Error Frequencies

Fig. 9.8 provides a histogram of all error values from the CFD model simulation for each turbine at each data point. The figure also provides a boxplot of the error values to more clearly represent statistical outliers. The CFD model required 30 – 60 minutes for each trial.

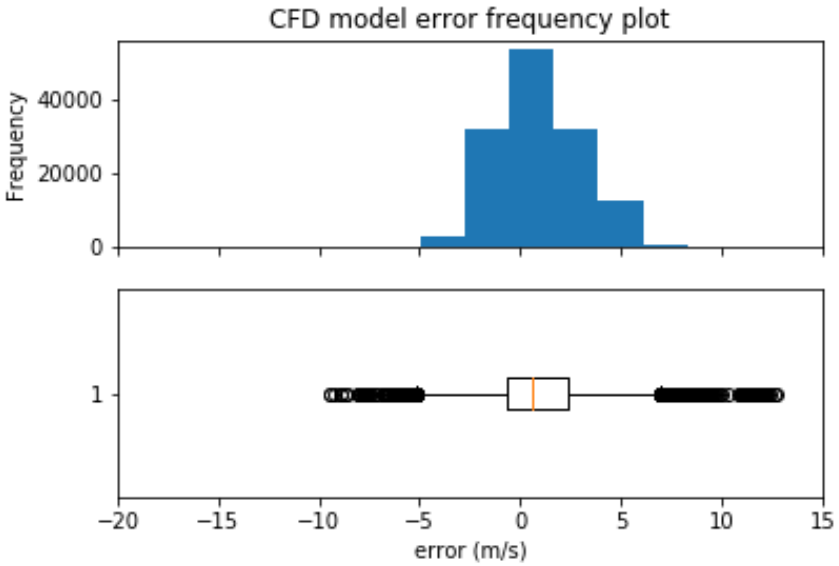

FIGURE 9.8: Histogram of Error from CFD Model Simulation

Figures 9.9 and 9.10 provide histograms of all error values from the Jensen model and Jensen model with NWP respectively. Each figure also includes a boxplot of the error values to more clearly represent statistical outliers. Both Jensen based models required 1 – 2 tenths of a second per trial.

Table 9.3 gives error distribution summary statistics for all data points by wake model. The root mean square error of all models are within 0.02 meters per second.

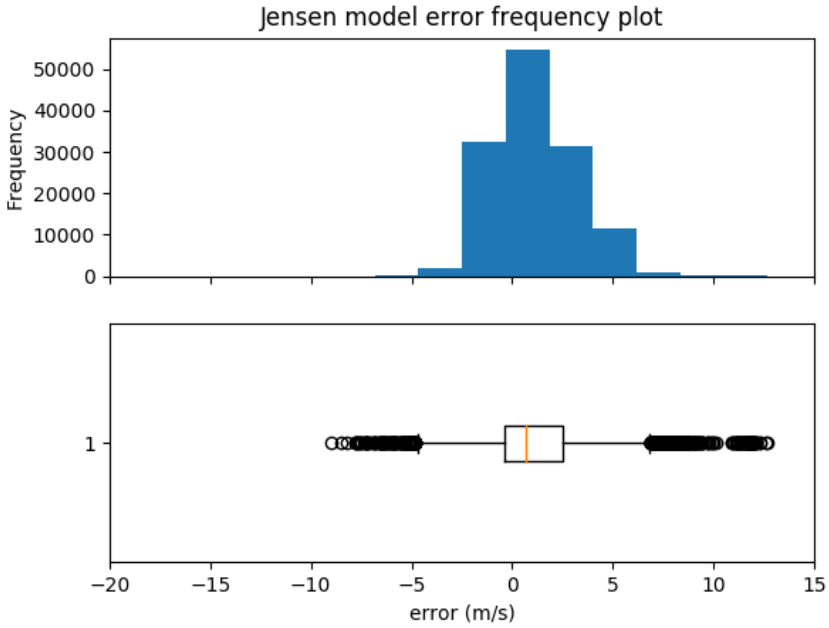

FIGURE 9.9: Histogram of Error from Jensen Model Simulation

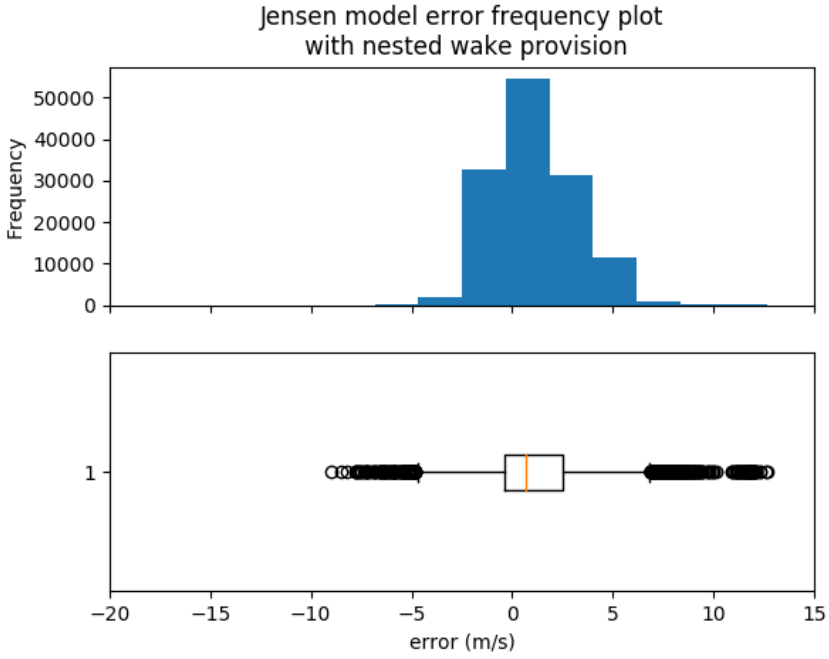

FIGURE 9.10: Histogram of Error from Jensen-NWP Model Simulation

TABLE 9.3: Summary of Wake Model Accuracy

Summarized error					
Model	RMSE	Mean Error	Standard Deviation	Median Error	IQR
CFD Model	2.319	0.907	2.134	0.630	3.035
Jensen Model	2.302	1.100	2.023	0.700	2.900
Jensen-NWP Model	2.300	1.096	2.022	0.700	2.900

Results Categorized by Wind Onset Angle

Table 9.4 gives a detailed analysis of each model's accuracy binned by wind onset angle. Analyses consider average error in meters per second (with negative values indicating model over-prediction), RMSE, and the percent of analyses in each category that resulted in under-prediction of turbine wind speeds. The skew towards over- or under-prediction is of particular importance in selecting appropriate models for optimization. The number of data points falling into each category are listed under "instances" for each onset angle.

Results Categorized by Ambient Wind Speed

Table 9.5 shows the analysis of each model's accuracy binned by ambient wind speed. As with the onset angle analysis, error is represented using average error in meters per second, RMSE, and the percent of analyses in each category that resulted in under-prediction of turbine wind speeds. The number of data points falling into each category are listed under "instances" for each wind speed.

TABLE 9.4: Results of simulation categorized by wind onset angle

Results by Wind Onset Angle									
average error ($\mathrm{m\,s^{-1}}$)									
wind onset angles	270	280	290	300	310	320	330	340	350
instances	104	140	244	369	507	734	761	467	286
CFD Model	0.435	0.513	0.695	0.908	0.957	0.822	0.376	0.304	0.409
Jensen Model	0.275	0.340	0.731	2.326	3.273	2.107	-0.096	-0.505	-0.128
Jensen-NWP Model	0.275	0.337	0.728	2.326	3.268	2.101	-0.102	-0.507	-0.130
RMSE									
wind onset angles	270	280	290	300	310	320	330	340	350
CFD Model	1.586	1.567	1.396	2.879	3.510	2.748	1.454	1.548	1.641
Jensen Model	1.422	1.455	1.422	2.881	3.611	2.828	1.216	1.336	1.504
Jensen-NWP Model	1.423	1.455	1.420	2.881	3.606	2.823	1.216	1.337	1.505
percent under-predicted									
wind onset angles	270	280	290	300	310	320	330	340	350
CFD Model	43.5	51.3	69.5	90.8	95.7	82.2	37.6	30.4	40.9
Jensen Model	50.4	54.0	73.4	92.0	97.0	86.2	41.4	30.1	40.9
Jensen-NWP Model	50.4	53.8	73.3	92.0	96.9	86.1	41.0	30.0	40.7

TABLE 9.5: Results of simulation categorized by ambient wind speed

Results by Ambient Wind Speed					
average error ($\mathrm{m\,s^{-1}}$)					
wind speeds ($\mathrm{m\,s^{-1}}$)	0 – 5	6 – 10	11 – 15	16 – 20	21 – 25
instances	620	1845	1,025	120	2
CFD Model	3.236	0.982	-0.317	-1.747	-3.219
Jensen Model	3.432	1.315	0.201	-1.038	-2.308
Jensen-NWP Model	3.423	1.297	0.174	-1.076	-2.360
RMSE					
wind speeds ($\mathrm{m\,s^{-1}}$)	0 – 5	6 – 10	11 – 15	16 – 20	21 – 25
CFD Model	3.623	2.110	1.516	2.396	3.652
Jensen Model	3.791	2.239	1.359	1.774	2.955
Jensen-NWP Model	3.783	2.229	1.353	1.792	2.993
percent under-predicted					
wind speeds ($\mathrm{m\,s^{-1}}$)	0 – 5	6 – 10	11 – 15	16 – 20	21 – 25
CFD Model	98.3	65.8	40.5	14.1	6.8
Jensen Model	98.8	72.6	50.9	20.5	8.1
Jensen-NWP Model	98.8	72.1	49.8	19.2	8.1

TABLE 9.6: Results of simulation categorized by number of upstream turbines

Results by Number of Upstream Turbines				
average error ($\mathrm{m\,s^{-1}}$)				
number of upstream turbines	0	1	2	3
CFD Model	1.045	0.542	0.868	0.639
Jensen Model	1.064	1.235	1.437	0.641
Jensen-CFD Model	1.064	1.235	1.394	0.641
RMSE				
number of upstream turbines	0	1	2	3
CFD Model	2.365	2.376	2.199	2.206
Jensen Model	2.325	2.038	2.286	1.477
Jensen-CFD Model	2.325	2.038	2.263	1.477
percent under-predicted				
number of upstream turbines	0	1	2	3
CFD Model	65.0	54.2	62.6	57.6
Jensen Model	63.0	76.0	77.1	65.8
Jensen-CFD Model	63.0	76.0	75.6	65.8

Results Categorized by Number of Upstream Turbines

Table 9.6 presents the analysis of each model's accuracy binned by the maximum number of upstream turbines present in each wind scenario. As with previous analyses, error is represented using average error in meters per second, RMSE, and the percent of analyses in each category that resulted in under-prediction of turbine wind speeds.

RMSE and Average Error Binned by Multiple Criteria

To better understand how the interactions between wind onset angle, wind speed, and the number of upstream turbines impact model error, I have separated the RMSE and average error of sections 9.1.2–9.1.2 into subcategories based on secondary binning criteria. As in earlier analyses, negative average error indicates model over prediction.

Figure 9.11a shows the RMSE of each model as a function of both wind speed and onset angle. Figure 9.11b shows the average error for each model under the same binning. All models indicate higher error with onset angles between 300 and 330 degrees. Additionally there is a spike in error magnitude for all models at an onset angle of 350 degrees and wind speeds of five meters per second or less. The CFD model also has a lower RMSE for all onset angles at wind speeds below $11\,\mathrm{m\,s^{-1}}$.

Examining Figure 9.11b, the CFD model consistently predicts wind speeds lower than those predicted by the Jensen model (average errors are consistently lower or more negative). Furthermore, the magnitude of the average error is inversely proportional to the ambient wind speed. As wind speeds increase, the models under predict by less, and eventually begin to over predict wind speeds. The lower wind speed predictions of the CFD model relative to either Jensen model result in higher accuracy at wind speeds below $11\,\mathrm{m\,s^{-1}}$. At higher wind speeds, the model begins over predicting leaving the Jensen models with smaller magnitude error. The spike in RMSE and average error at low wind speeds from a 350 degree onset angle is a highlighted in Figure 9.11a, and likely results from inaccurate and insufficient data. Four of the 3,612 data points fit into this category. The nacelle anemometers reported wind speeds greater than twice the met tower wind speeds at two of those data points.

Figure 9.12 shows the RMSE and average error of each model binned by wind speed and the number of upstream turbines. Figure 9.11a shows the CFD model more accurately predicting turbine wind speeds at ambient speeds less than $11\,\mathrm{m\,s^{-1}}$, however as wind

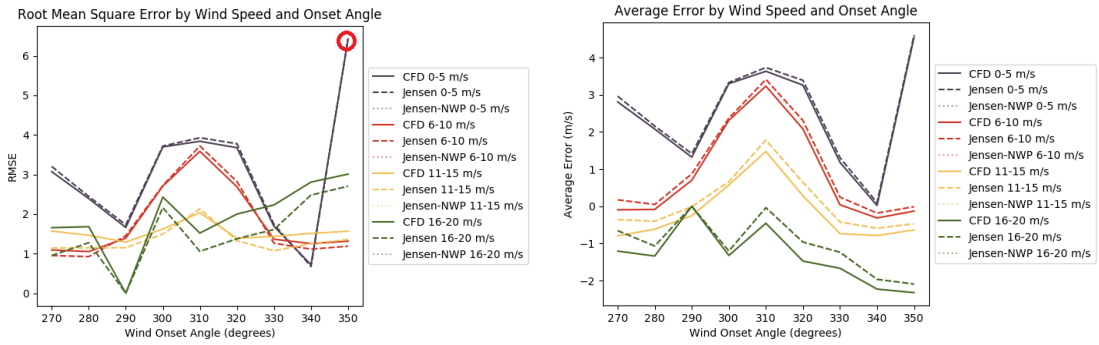

(a) RMSE

(b) Average Error (negative error represents model over prediction)

FIGURE 9.11: Model Error by Wind Speed and Onset Angle

speeds increase the Jensen models begin to outperform the CFD model. Figure 9.11b shows that both models have similar average error with zero or three upstream turbines, but diverge in error with one or two upstream turbines. The difference in error between models increases with increased wind speed, and once again we see an inverse relationship between ambient wind speed and average error. This relationship once again results in smaller error of the Jensen models relative to the CFD models at high wind speeds.

Figure 9.13 gives the RMSE and average error of each model as a function of wind onset angle and the number of upstream turbines. In this figure, zero RMSE and average error indicate that no values fit within the subcategory (eg., there were no values at a 310 degree onset angle with three upstream turbines). For numbers of upstream turbines with data points at every onset angle, the general shape of the RMSE is similar to that of Figure 9.11a, with increased error in the 300–320 degree range of onset angles. The CFD has a lower RMSE then either Jensen model in this range. Below 290 degrees and above 330 degrees, there is more variation in relative RMSE between models, with no model showing consistantly better accuracy at all wind speeds. Figure 9.11b shows the Jensen model predicting lower wind speeds than the CFD model under most conditions.

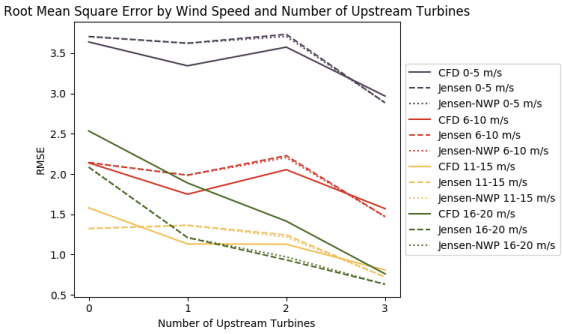

(a) RMSE

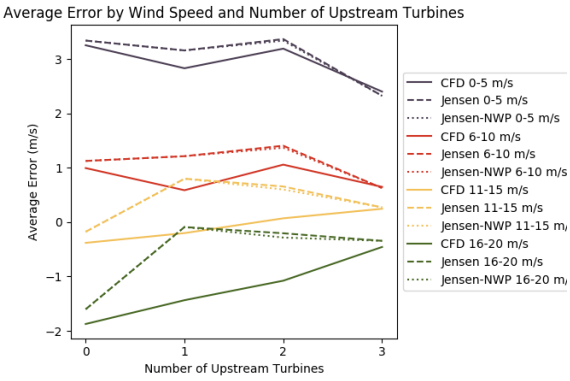

(b) Increasing Average Error with Increasing Wind Speed (negative error represents model over prediction)

FIGURE 9.12: Model Error by Wind Speed and Number of Upstream Turbines

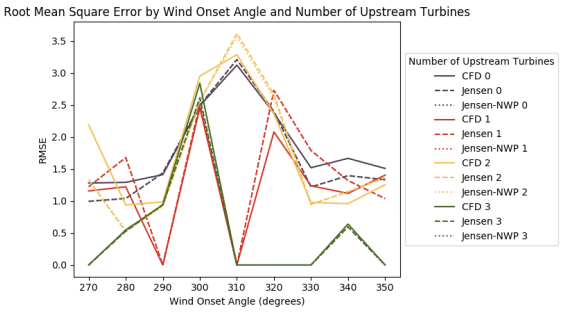

(a) RMSE

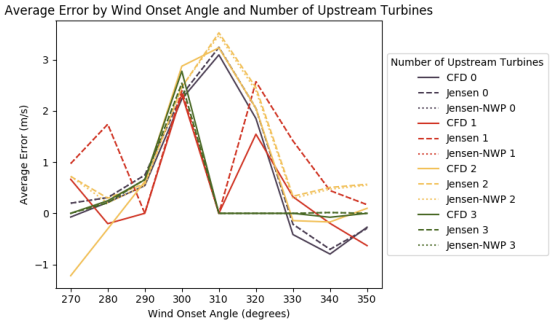

(b) Average Error (negative error represents model over prediction)

FIGURE 9.13: Model Error by Wind Onset Angle and Number of Upstream Turbines

9.2 Wake Model Selection Discussion

9.2.1 Relative Response of Wake Models Discussion

Under both power scenarios, the CFD model shows non-monotonic power development by the upstream turbine at small turbine spacing. The downstream turbine in these tests exhibited similar relative trends under both power development scenarios, with a slight leftward shift corresponding to the sub-optimal development conditions. In these tests, the Jensen model under-predicts power development when compared to the CFD model under smaller turbine spacing, and over predicts power development with larger spacing. These trends were largely unchanged when incorporating a third downstream turbine.

In examining the results of the hard-coded layouts, the nested wake provision allows for closer alignment between the Jensen and CFD wake model for small quantities of nested wakes, but seems to over correct wind speeds relative to the CFD model, resulting in larger disparities in modeled output with increasing numbers of nested wakes.

9.2.2 Absolute Accuracy Analysis for Wake Models Discussion

As shown in Table 9.3, the results of the Jensen model simulations with and without the nested wake provision are very similar. This similarity makes sense logically as the provision applied to only a few of the turbines in the field. However, the error of the CFD model was remarkably similar to that of either Jensen model. The CFD model resulted in slightly smaller average and slightly larger root mean square errors, signifying slight model over-prediction relative to the Jensen models.

The CFD model frequently produced a smaller average error than either Jensen model, this tendency is best explained through an examination of the error binned by winds speed. In Figure 9.5 one can see that all three models had a tendency to over-predict wind speeds as wind speeds increased, however the CFD model consistently predicted a

wind speed value higher than that predicted by either Jensen model (the average errors from the CFD evaluation were more negative). This phenomenon is mirrored in the rows indicating the percentage of values that under-predicted wind speeds. Because the Jensen models predicted lower wind speeds overall, they had a larger percentage of under-predicted values in wind speed bins with large numbers of data points.

It is important to remember that these results are a comparison of a two dimensional CFD model with a two dimensional extrapolation of the Jensen model. Incorporating three dimensional models may increase the discrepancy between model outputs and increase the accuracy of the CFD model in particular.

10 TURBINE AVAILABILITY ANALYSIS RESULTS AND DISCUSSION

This chapter contains proprietary data and as such was omitted from the final thesis submission with permission from the Oregon State Graduate School.

11 CONCLUSIONS

The purpose of this research was to address cost-related barriers to wind farm development with an emphasis on floating offshore analysis off the US Pacific coast. US offshore wind energy markets have lagged behind those of Europe, however the large US resource combined with optimized turbine layouts can expand the profitability of US wind, producing a prime location for offshore development.

Chapter 6 gave a comparison of optimization algorithms applied to the offshore wind farm layout problem under a simplified, unidirectional wind case. This analysis indicated that an extended pattern search has superior optimization abilities with fewer objective evaluations and time requirements than a genetic algorithm or particle swarm optimization given similar optimization and environmental settings. The results of this study led me to use the extended pattern search throughout subsequent optimizations.

To further validate the performance of the EPS against existing literature, Chapter 6 includes a comparison to layouts obtained by Liu and Wang using an Adapted GA. For 16-turbine layouts, both the EPS and Adapted GA generated 100% efficient layouts in a 4 km x 4 km field. The EPS also generated 100% efficient layouts for farms containing up to 34 turbines.

Chapters 7 and 8 implement the EPS from Chapter 6 to optimize onshore and offshore turbine layouts under unidirectional and multidirectional wind cases, respectively. The objective function minimized the total farm cost per kilowatt and levelized cost of energy using advanced models to properly represent cost, wake interactions, and power production across wind farms.

The optimized offshore layout had a cost per kilowatt of $20,400 with 21 turbines. Plotting the number of turbines considered against the optimized offshore final objective evaluation showed decreasing evaluations until near-100% efficient layouts were no longer

possible. These findings were reinforced by the results of multidirecetional offshore optimization, with an optimal cost per kilowatt of $14,821.

Similar trends could be seen in the results of onshore simulation, except rather than decreasing the objective with more turbines, the evaluation remained constant until near 100% efficient layouts could no longer be achieved. The optimized onshore layout was found to have a cost per kilowatt of approximately $16,362 under unidirectional wind conditions, which could be achieved with 18 or fewer turbines. These results highlight the optimization ramifications of onshore and offshore cost structures.

Chapter 9 details the trade-offs between a high-fidelity CFD wake model and two versions of a commonly used linearized wake model in farm analysis. The CFD model did not produce a statistically significant reduction of root mean square error in wind speed estimation when compared to either Jensen model analyzed. It is not clear from this experiment whether discrepancies in error are a result of erroneous data values or model error. There is no clear indication that a 2D CFD model is useful in the optimization step of wind farm development.

Chapter 10 compares the performance of turbines from two different manufacturers on the basis of energetic availability and as a function of six different environmental conditions. Following the comparison of energetic availability, a secondary study was conducted to better understand the causes of availability loss. Vendor A asset losses resulting in corrective maintenance needs were twice that of Vendor B asset losses. Losses related to substations and the electric grid were both small in magnitude and similar for the fleets of Vendor A and B turbines.

Turbine stoppage events requiring corrective maintenance were further analyzed to better understand which turbine components were contributing the greatest generation losses. Vendor A turbines showed disproportionately large losses related to control, hydraulic, and yaw systems when compared to Vendor B turbines. Vendor B turbines showed

larger relative losses associated with the pitch controllers, the main gearbox, and the blade pitch actuators.

The results of these studies may be used by wind farm developers to advance onshore and offshore farm modeling and optimization. Chapter 6 indicates that an extended pattern search may produce consistently better layouts in less time than other heuristic optimization approaches. Chapters 7 and 8 compare optimization trends for onshore and offshore wind farms in simplified and realistic wind cases. Chapter 9 quantifies the trade-offs between accuracy and computational expense of common wake models, indicating that simplistic linearized wake models may be adequate in wind farm optimization. Finally, Chapter 10 explores performance differences between individual turbine manufacturers, indicating that discrepancies in turbine quality between manufacturers may have a significant impact on lifetime farm profitability.

12 FUTURE WORK

12.1 Optimization using CFD Wake Model

While improvements in accuracy of the CFD model relative to the analytical Jensen model were relatively small in the particular turbine layout presented in this work, higher-fidelity wake modeling may have larger ramifications on the optimization of turbine layouts. Full-scale optimization with the CFD wake model, particularly if the model was expanded into three dimensions, may provide new insight into layout optimization.

12.2 Three-Dimensional CFD Analysis

The CFD wake model used in this research simplified the field into a two-dimensional plane at turbine hub height. I used a two-dimensional Jensen model to compare results of optimization against the two-dimensional CFD model, however results of the wake model selection study may vary considerably if three-dimensional CFD and Jensen models were used.

12.3 Optimization with Non-uniform Turbines

While most wind farms incorporate only one turbine type, existing literature has shown that incorporating several turbine types with different hub heights and rotor radii may increase the energy generation of a farm [50]. A logical future step in this research would be to incorporate a sub-search for turbine type optimization into the existing extended pattern search in order to fully understand differences in optimized layouts onshore and offshore.

BIBLIOGRAPHY

1. H. Bailey, B. Brookes, and P. Thompson, "Assessing environmental impacts of offshore wind farms: lessons and recommendations for the future," *Aquatic Biosystems*, vol. 10, 2014.

2. C. Forinash and B. DuPont, "Optimization of Floating Offshore Wind Energy Systems Using an Extended Pattern Search Method," *ASME 2016 International Design Engineering Technical Conferences and Computers and Information in Engineering Conference*, pp. 1–11, 2016.

3. A. Miller, C. Forinash, and B. DuPont, "An extended pattern search approach for optimizing offshore floating wind farms," Under Review, 2017.

4. B. L. DuPont, J. Cagan, and P. Moriarty, "Optimization of wind farm layout and wind turbine geometry using a multi level extended pattern search algorithm that accounts for variation in wind shear profile shape," in *Proceedings of the ASME 2012 International Design Engineering Technical Conferences & Computers and Information in Engineering Conference*, 2010, pp. 243–252.

5. U.S. Energy Information Administration, "International energy outlook 2017 overview," web, 2017.

6. Energy Information Administration, "U.S. energy consumption by energy source, 2016."

7. American Wind Energy Association, "Wind energy facts at a glance." [Online]. Available: https://www.awea.org/wind-energy-facts-at-a-glance

8. United States Department of Energy, "20% Wind Energy by 2030 Increasing Wind Energy's Contribution to U.S. electricity Supply," *Vasa*, p. 248, 2008.

9. M. Schwartz, D. Heimiller, and S. Haymes, "Assessment of Offshore Wind Energy Resources for the United States," National Renewable Energy Laboratory, Tech. Rep. June, 2010.

10. P. Sclavounos, "Floating Offshore Wind Turbines," *Marine Technology Society Journal*, vol. 42, no. 2, pp. 39–43, 2008.

11. B. Byrne and G. Houlsby, "Foundations for offshore wind turbines," *Philosophical Transactions. Series A, Mathematical, physical, and engineering sciences*, vol. 361, no. 2003, pp. 2909–2930, 2003.

12. D. Roddier, C. Cermelli, A. Aubault, and A. Weinstein, "WindFloat: A floating foundation for offshore wind turbines," *Journal of Renewable and Sustainable Energy*, vol. 2, no. 3, p. 033104, 2010.

13. R. O'Neil, "Oregon Department of Energy Marine Transmission in Oregon Report to Oregon Legislature," Oregon Department of Energy, Tech. Rep., 2014.

14. Principle Power, "U.S. Department of Energy Supports Oregon Offshore Wind with Grant Accelerating Development of WindFloat Pacific Project," Press Release, 2014.

15. C. N. Elkinton, J. F. Manwell, J. G. Mcgowan, and R. Energy, "Offshore Wind Farm Layout Optimization (OWFLO) Project: Preliminary Results," *44th AIAA Aerospace Sciences Meeting and Exhibit, Reno, Nevada, Jan. 2006*, pp. 1–9, 2006.

16. C. Elkinton, J. Manwell, and J. McGowan, "Algorithms for Offshore Wind Farm Layout Optimization," *Wind Engineering*, vol. 32, no. 1, pp. 67–84, 2008.

17. C. Forinash and B. DuPont, "Optimization of Floating Offshore Wind Energy Systems Using an Extended Pattern Search Method," *35th International Conference on Ocean Offshore & Arctic Engineering*, pp. 1–11, 2016.

18. M. Mahdy and A. S. Bahaj, "Multi criteria decision analysis for offshore wind energy potential in egypt," *Renewable Energy*, vol. 118, pp. 279–289, 2018.

19. P. M. Soares, D. C. Lima, R. M. Cardoso, M. L. Nascimento, and A. Semedo, "Western iberian offshore wind resources: More or less in a global warming climate?" *Applied Energy*, vol. 203, pp. 72–90, 2017.

20. P.-C. Chang and C.-M. Lai, "Wind resource analysis and optimization of offshore wind farm layout in the central taiwan," in *IEEE International Conference on Smart Grid and Smart Cities*, 2017.

21. M. Satir and F. M. an Kevin McDonnell, "Feasibility study of an offshore wind farm in the aegean sea, turkey," *Renewable and Sustainable Energy Reviews*, vol. 81, pp. 2552–2562, 2018.

22. N. Kirchner-Bossi and F. Porté-Agel, "Wind farm layout optimization through a crossover-elitist evolutionary algorithm performed over a high performing analytical wake model," in *19th EGU General Assembly*, April 2017.

23. A. P. Stanley, J. Thomas, A. Ning, J. Annoni, K. Dykes, and P. Fleming, "Gradient-based optimization of wind farms with different turbine heights," in *American Institute of Aeronautics and Astronautics SciTech*, 2017.

24. R. N. King, K. Dykes, P. Graf, and P. E. Hamlington, "Optimization of wind plant layouts using an adjoint approach," *Wind Energy Science*, vol. 2, pp. 115 – 131, 2017.

25. X. Gao, H. Yang, and L. Lu, "Investigation into the optimal wind turbine layout patterns for a Hong Kong offshore wind farm," *Energy*, vol. 73, no. June 2015, pp. 430–442, 2014.

26. X. Gao, H. Yang, L. Lin, and P. Koo, "Wind turbine layout optimization using multi-population genetic algorithm and a case study in Hong Kong offshore," *Journal of Wind Engineering and Industrial Aerodynamics*, vol. 139, pp. 89–99, 2015.

27. P. E. Réthoré, P. Fuglsang, G. C. Larsen, T. Buhl, T. J. Larsen, and H. A. Madsen, "TOPFARM: Multi-fidelity optimization of wind farms," *Wind Energy*, vol. 17, no. 12, pp. 1797–1816, 2014.

28. F. Liu and Z. Wang, "Offshore Wind Farm Layout Optimization Using Adapted Genetic Algorithm: A different perspective," *CoRR*, 2014.

29. R. A. Rivas, J. Clausen, K. S. Hansen, and L. E. Jensen, "Solving the Turbine Positioning Problem for Large Offshore Wind Farms by Simulated Annealing," *Wind Engineering*, vol. 33, no. 3, pp. 287–297, 2009.

30. S. Salcedo-Sanz, D. Gallo-Marazuela, A. Pastor-Sánchez, L. Carro-Calvo, A. Portilla-Figueras, and L. Prieto, "Offshore wind farm design with the Coral Reefs Optimization algorithm," *Renewable Energy*, vol. 63, pp. 109–115, 2014.

31. C. M. Ituarte-Villarreal and J. F. Espiritu, "Optimization of wind turbine placement using a viral based optimization algorithm," *Procedia Computer Science*, vol. 6, pp. 469–474, 2011.

32. G. Mosetti, C. Poloni, and D. Diviacco, "Optimization of wind turbine positioning in large wind farms by means of a genetic algorithm," *Journal of Wind Engineering and Industrial Aerodynamics*, 1994.

33. S. F. Rodrigues, R. Teixeira Pinto, M. Soleimanzadeh, P. A. N. Bosman, and P. Bauer, "Wake losses optimization of offshore wind farms with moveable floating wind turbines," *Energy Conversion and Management*, vol. 89, pp. 933–941, 2015.

34. P. Guérivière, "Press Release Ideol Announces a New Floating Platform Solution To Accelerate the Deployment of Offshore Wind Farms, La Ciotat, France," IDEOL, Tech. Rep., 2011.

35. B. Pérez, R. Minguez, and R. Guanche, "Offshore wind farm layout optimization using mathematical programming techniques," *Renewable Energy*, vol. 53, pp. 389–399, 2013.

36. B. DuPont, J. Cagan, and P. Moriarty, "An advanced modeling system for optimization of wind farm layout and wind turbine sizing using a multi-level extended pattern search algorithm," *Energy*, vol. 106, pp. 802–814, 2016.

37. B. DuPont and J. Cagan, "An Extended Pattern Search Approach to Wind Farm Layout Optimization," *Journal of Mechanical Design*, vol. 134, no. August 2012, p. 081002, 2012.

38. B. L. DuPont and J. Cagan, "Multi-Stage Optimization of Wind Farms with Limiting Factors," *ASME International Design Engineering Technical Conferences and Computers and Information in Engineering Conference*, pp. 1–12, 2013.

39. B. L. DuPont, J. Cagan, and P. Moriarty, "Optimization of Wind Farm Layout and Wind Turbine Geometry Using a Multi-Level Extended Pattern Search Algorithm That Accounts for Variation in Wind Shear Profile Shape," *38th Design Automation Conference*, vol. 3, Parts A and B, p. 243, 2012.

40. S. Yin and J. Cagan, "An Extended Pattern Search Algorithm for 3D Component Layout," *Journal of Mechanical Design*, vol. 122, no. 1, pp. 102–108, 2000.

41. A. L. Manwell, J. F., McGowan, J. G., and Rogers, *Wind Energy Explained: theory, design, and application.* West Sussex, UK: John Wiley & Sons Ltd., 2009.

42. R. J. Barthelmie, L. Folkerts, G. C. Larsen, K. Rados, S. C. Pryor, S. T. Frandsen, B. Lange, and G. Schepers, "Comparison of wake model simulations with offshore wind turbine wake profiles measured by sodar," *Journal of Atmospheric and Oceanic Technology*, September 2005.

43. N. O. Jensen, "A note on wind generator interaction," *Risø-M-2411 Risø National Laboratory Roskilde*, pp. 1–16, 1983. [Online]. Available: http://www.risoe.dk/rispubl/VEA/veapdf/ris-m-2411.pdf

44. B. L. DuPont, "Exploring the application of an advanced extended pattern search algorithm within a multi-agent system to wind farm optimization," Ph.D. dissertation, Carnegie Mellon University, 2013.

45. National Renewable Energy Laboratory, "WindSE2D [Computer Software] v2.0," Prepublication Release, 2017.

46. L. Fingersh, M. Hand, and A. Laxson, "Wind Turbine Design Cost and Scaling Model," NREL, Tech. Rep. TP-500-40566, 2006.

47. k. Deb, A. Pratap, and S. Agarwal, "A fast and elitist multiobjective genetic algorithm: NSGA-II," *IEEE Transactions on Evolutionary Computation*, vol. 6, 2002.

48. D. Hsu, S., Meindl, E., Gilhousen, "Determining the Power-Law Wind-Profile Exponent under Near-Neutral Stability Conditions at Sea," *Journal of Applied Meteorology*, vol. 33, 1994.

49. S. Grady, M. Hussaini, and M. Abdullah, "Placement of wind turbines using genetic algorithms," *Renewable Energy*, 2005.

50. S. Chowdhury, J. Zhang, A. Messac, and L. Castillo, "Optimizing the arrangement and the selection of turbines for wind farms subject to varying wind conditions," *Renewable Energy*, vol. 52, pp. 273–282, 2013.